

Multiview Differential Geometry of Curves

Ricardo Fabbri · Benjamin B. Kimia

Abstract The field of multiple view geometry has seen tremendous progress in reconstruction and calibration due to methods for extracting reliable point features and key developments in projective geometry. Point features, however, are not available in certain applications and result in unstructured point cloud reconstructions. General image curves provide a complementary feature when keypoints are scarce, and result in 3D curve geometry, but face challenges not addressed by the usual projective geometry of points and algebraic curves. We address these challenges by laying the theoretical foundations of a framework based on the differential geometry of general curves, including stationary curves, occluding contours, and non-rigid curves, aiming at stereo correspondence, camera estimation (including calibration, pose, and multiview epipolar geometry), and 3D reconstruction given measured image curves. By gathering previous results into a cohesive theory, novel results were made possible, yielding three contributions. First we derive the differential geometry of an image curve (tangent, curvature, curvature derivative) from that of the underlying space curve (tangent, curvature, curvature derivative, torsion). Second, we derive the differential geometry of a space curve from that of two corresponding image curves. Third, the differential motion of an image curve is derived from camera motion and the differential geometry and motion of the space curve. The availability of such a theory enables novel curve-based multiview reconstruction and camera estimation systems to augment existing point-based approaches. This theory has been used to reconstruct a “3D curve sketch”, to determine camera pose from local curve geometry, and tracking; other developments are underway.

Keywords Structure from Motion · Multiview Stereo · Torsion · Non-Rigid Space Curves

1 Introduction

The automated estimation of camera parameters and the 3D reconstruction from multiple views is a fundamental problem in computer vision. These tasks rely on correspondence of image structure commonly in the form of keypoints, although dense patches and curves have also been used. **Keypoint-based methods** extract point features designed to be stable with view variations. They

Brown University, Division of Engineering, Providence RI 02912, USA. **Draft date:** April 29, 2016 00:29
E-mail: {rfabbri,kimia}@lems.brown.edu

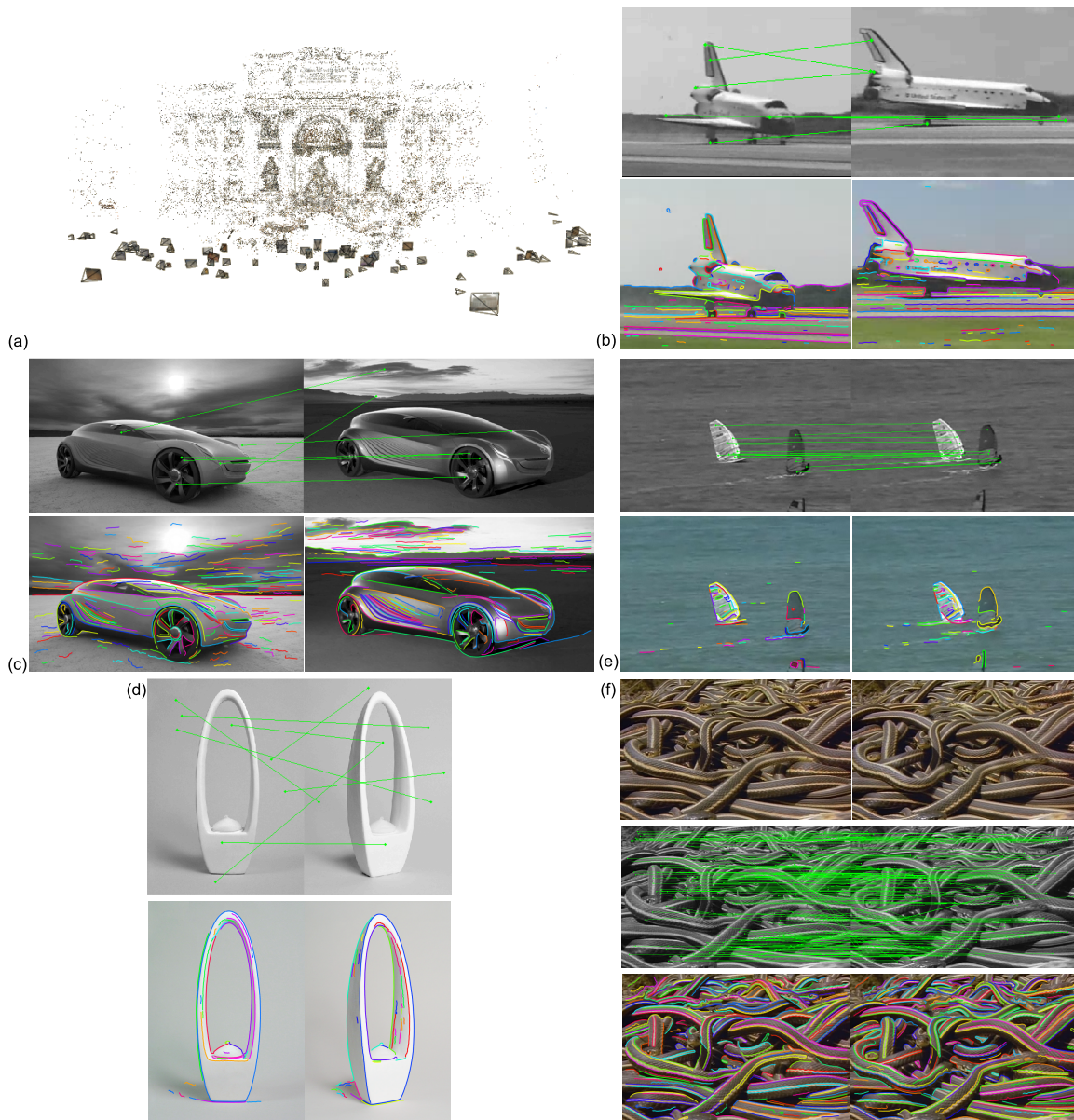


Fig. 1: (a) Keypoint-based approaches give a sparse point cloud reconstruction (Agarwal et al 2009; Heinly et al 2015) which can be made richer, sharper, and denser with curve structure. (b) Wide baseline views not sharing interest points often share curve structure. (c,d) Not enough points matching views of homogenous objects with sufficient curve structure. (e) Each moving object or non-rigid object requires its own set of features, but may not have enough texture.

satisfy certain local conditions in the spatial and scale dimensions (Mikolajczyk and Schmid 2004; Harris and Stephens 1988; Moravec 1977; Lowe 2004), and are attributed with a local description of the image (Mikolajczyk and Schmid 2005). While many of these points are not stable with view changes in that they disappear/appear or vary abruptly, many are stable enough for matching with

RANSAC (Fischler and Bolles 1981) to initialize camera models for bundle adjustment (Hartley and Zisserman 2000; Pollefeys et al 2004; Agarwal et al 2009; Heinly et al 2015; Diskin and Asari 2015).

A major drawback of interest points is their sparsity compared to the curves and surfaces composing the scene, producing a cloud of 3D points where geometric structure is not explicit, Figure 1(a). This is less of a problem for camera estimation (Agarwal et al 2009), but in applications such as architecture, industrial design, object recognition, and robotic manipulation, explicit 3D geometry is required. Moreover, meshing unstructured point clouds produces oversmoothing (Kazhdan et al 2006; Furukawa and Ponce 2010). These techniques are therefore inadequate for man-made environments (Simoes et al 2012) and objects such as cars (Shinozuka and Saito 2014), non-Lambertian surfaces such as that of the sea, appearance variation due to changing weather (Baatz et al 2012), and wide baseline (Moreels and Perona 2007), Figure 1(b). We claim that by using even *some* curve information the 3D reconstruction can be made more structurally rich, sharper and less sparse.

The use of keypoints requires an abundance of features surviving the variations between views. While this occurs for many scenes, in many others this is not the case, such as (i) homogeneous regions from man-made objects, Figure 1(c,d); (ii) moving objects require their own set of features which are too few without sufficient texture, Figure 1(e); (iii) non-rigid objects require a rich set of features per local patch, Figure 1(f). While curve features, like keypoints, may not be abundant the interior of highly homogeneous regions or in nonrigid or small moving objects, *curves rely on texture to a much lesser extent*, as shown in Figure 1(c,d,e); the boundary of homogeneous regions are good cues (often the *only* cues), enabling extracting information structure and motion. In all these situations, there may be sufficient curvilinear structure, Figure 1, motivating augmenting the use of interest points with curves.

Pixel-based multiview stereo relies on matching intensities across views, resulting in a dense point cloud or a mesh reconstruction. This produces detailed 3D reconstructions of objects imaged under controlled conditions by a large number of precisely calibrated cameras (Furukawa and Ponce 2007; Habbecke and Kobbelt 2007; Hernández Esteban and Schmitt 2004; Goesele et al 2007; Seitz et al 2006; Calakli et al 2012; Restrepo et al 2014). However, there are a number of limitations: they typically assume that the scene consists of a single object or that objects are of a specific type, such as a building; they often require accurate camera calibration and operate under controlled acquisition; and they need to be initialized by the visual hull of the object or a bounded 3D voxel volume, compromising applicability for general scenery.

Curve-based multiview methods can be divided into three categories: (i) convex hull construction, (ii) occluding contour reconstruction, and (iii) use of differential geometry in binocular and trinocular stereo. First, when many views are available around an object, a visual hull has been constructed from silhouette curves and then evolved to optimize photometric constraints while constraining the projection to the silhouettes. The drawbacks are similar to those of pixel-based multiview stereo. Second, the occluding contours extracted from frames of a video have been used to reconstruct a local surface model given the camera parameters for each frame. These methods require highly controlled acquisition and image curves that are easy to segment and track. In addition, since only silhouettes are used, internal surface variations which may not map to apparent contours in any view will not be captured, *e.g.*, surface folds of a sculpture.

Third, some methods employ curve differential geometry in correlating structure across views. Complete 3D reconstruction pipelines based on straight lines (Lebeda et al 2014; Zhang 2013; Fathi et al 2015), algebraic and general curve features (Teney and Piater 2012; Litvinov et al 2012; Fabbri and Kimia 2010; Fabbri et al 2012; Pötsch and Pinz 2011) have been proposed. The compact curve-based 3D representation that has found demand in several tasks: fast recognition of general 3D

scenery (Pötsch and Pinz 2011), efficient transmission of general 3D scenes, scene understanding and modeling by reasoning at junctions (Mattingly et al 2015), consistent non-photorealistic rendering from video (Chen and Klette 2014), modeling of branching structures, to name a few (Rao et al 2012; Kowdle et al 2012; Wang et al 2014).

Related work: Differential geometry does not provide hard constraints for matching in static binocular stereo, as known for tangents and curvatures (Robert and Faugeras 1991), and shown here for higher order. Heuristics have been employed in short baseline to limit orientation difference (Arnold and Binford 1980; Grimson 1981; Sherman and Peleg 1990), to match appearance via locally planar approximations (Schmid and Zisserman 2000), or to require 3D curve reconstructions arising from two putative correspondence pairs to have minimum torsion (Li and Zucker 2003). When each stereo camera provides a video and the scene (or stereo head) moves rigidly, differential geometry provides a hard constraint (Faugeras and Papadopoulou 1993; Papadopoulou 1996; Faugeras and Papadopoulou 1992). Differential geometry is more directly useful in trinocular and multiview stereo, as pioneered by Ayache and Lustman (1987), due to the constraint that corresponding pairs of points and tangents from two views uniquely determine a point and tangent in a third to match line segments obtained from edge linking (Ayache and Lustman 1987; Spetsakis and Aloimonos 1991; Shashua 1994; Hartley 1995). Robert and Faugeras (1991) extended this to include curvature: 3D curvature and normal can be reconstructed from 2D curvatures at two views, determining the curvature at a third. The use of curvature improved reconstruction precision and density, with heuristics such as the ordering constraint (Ohta and Kanade 1985). Schmid and Zisserman (2000) derived multiview curvature transfer when only the trifocal tensor is available, by a projective-geometric approach to the osculating circle as a conic.

Curves have also been employed for camera estimation using the concept of epipolar tangencies: corresponding epipolar lines are tangent to a curve at corresponding points (Cipolla and Giblin 1999; Astrom et al 1999; Astrom and Kahl 1999; Kahl and Heyden 1998; Porrill and Pollard 1991; Kaminski and Shashua 2004; Berthilsson et al 2001; Wong et al 2001; Mendonça et al 2001; Wong and Cipolla 2004; Furukawa et al 2006; Hernandez et al 2007; Cipolla et al 1995; Reyes and Bayro Corrochano 2005; Sinha et al 2004). This is used to capture epipolar geometry or relative pose.

Curve-Based Multiview Geometry: What would be desirable is a generally applicable framework, *e.g.*, a handheld video acquiring images around objects or a set of cameras monitoring a scene, where image curve structure can be used to estimate camera parameters and reconstruct a 3D curve sketch on which a surface can be tautly stretched like a tent on a metallic scaffold. This paper provides the *mathematical foundation* for this curve-based approach. Image curve fragments are attractive because they have good localization, have greater invariance than interest points to changes in illumination, are stable over a greater range of baselines, and are denser than interest points. Moreover, for the special case of occluding contours, dense 3D surface patch reconstructions are available. The notion that image curves contain much of the image information is supported by recent studies (Koenderink et al 2013; Zucker 2014; Kunsberg and Zucker 2014; Cole et al 2009).

This paper develops the theoretical foundations for using the differential geometry of image curve structure as a complementary alternative to interest points. This paper is organized along the lines of these questions: *(i)* How does the differential geometry of a space curve map to the differential geometry of the image curve it projects to? *(ii)* How can the differential geometry of a space curve be reconstructed from that of two corresponding image curves? *(iii)* How does the differential geometry of an image curve evolve under camera motion? Section 2 establishes notation for image and space curves, camera projection and motion, and discusses the distinction between *stationary* and *non-stationary* 3D contours. Section 3 relates the differential geometry of image curves, *i.e.*, tangent,

curvature, and curvature derivative from the differential geometry of the space curves they arise from, *i.e.*, tangent and normal, curvature, torsion, and curvature derivatives. Section 4 derives the differential geometry of a space curve at a point from that at two corresponding image curve points showing the key result that the ratio of parametrization speeds is an intrinsic quantity. The key new result is the reconstruction of torsion and curvature derivative, given corresponding differential geometry in two views. Section 5 considers differential camera motion and relates the differential geometry of a space curve to that of the image and camera motion. Results are provided concerning image velocities and accelerations with respect to time for different types of curves; in particular, distinguishing apparent and stationary contours requires second-order time derivatives (Cipolla and Giblin 1999). We study the spatial variation of the image velocity field along curves, which can be useful for exploiting neighborhood consistency of velocity fields along curves. The main new result generalizes a fundamental curve-based differential structure from motion equation (Papadopoulo and Faugeras 1996; Papadopoulo 1996) to occluding contours.

This paper integrates the above results under the umbrella of a unified formulation and completes missing relationships. As a generalized framework, it is expected to serve as reference for research relating local properties of general curves and surfaces to those of cameras and images. Much of this has already been done, but a considerable amount has not, as mentioned earlier, and most results are scattered in the literature. This theoretical paper has been the foundation of practical work already reported on reconstruction and camera estimation systems as follows. First, the pipeline for the reconstruction of a 3D Curve Sketch from image fragments in numerous views (Fabbri and Kimia 2010; Usumezbas et al 2016) relies on the results on 3D reconstruction and projection of differential geometry reported in this paper, and a future extension of this pipeline would require most results in this paper. Second, a recent practical algorithm for pose estimation based on differential geometry of curves (Fabbri et al 2012) relies on the theory reported in this paper, treating the camera pose as unknowns and using differential geometry to solve for them, *cf.* ensuing efforts by Kuang and Åström (2013); Kuang et al (2014). Third, work on differential camera motion estimation from families of curves based on the present work has been explored by Jain (2009); Jain et al (2007b,a). These works are currently under intense development in order to build a complete structure from motion pipeline based on curves, which would use the majority of the results described in this paper, including analogous results for multiview surface differential geometry that are under development.

2 Notation and Formulation

2.1 Differential Geometry of Curves

For our purposes, a 3D space curve Γ is a smooth map $S \mapsto \mathbf{I}^w(S)$ of class C^∞ from an interval of \mathbb{R} to \mathbb{R}^3 , where S is an arbitrary parameter, \tilde{S} is the arc-length parameter, and the superscript w denotes the world coordinates. The local Frenet frame of Γ in world coordinates is defined by the unit vectors tangent \mathbf{T}^w , normal \mathbf{N}^w , binormal \mathbf{B}^w ; G is speed of parametrization, curvature K , and torsion τ . Similarly, a 2D curve γ is a map $s \mapsto \boldsymbol{\gamma}(s)$ of class C^∞ from an interval of \mathbb{R} to \mathbb{R}^2 , where s is an arbitrary parameter, \tilde{s} is arc-length, g is speed of parametrization, \mathbf{t} is (unit) tangent, \mathbf{n} is (unit) normal, κ is curvature, and κ' is curvature derivative. We will be concerned with regular curves, so that $G \neq 0$ and $g \neq 0$ unless otherwise stated. By classical differential geometry (do Carmo

1976), we have

$$\left\{ \begin{array}{l} G = \|\mathbf{T}^{w'}\| \\ \mathbf{T}^w = \frac{\mathbf{T}^{w'}}{G} \\ K = \frac{\|\mathbf{T}^{w'}\|}{G} \end{array} \right. \quad \mathbf{N}^w = \frac{\mathbf{T}^{w'}}{\|\mathbf{T}^{w'}\|} \quad \mathbf{B}^w = \mathbf{T}^w \times \mathbf{N}^w \quad \left[\begin{array}{l} \mathbf{T}^{w'} \\ \mathbf{N}^{w'} \\ \mathbf{B}^{w'} \end{array} \right] = G \left[\begin{array}{ccc} 0 & K & 0 \\ -K & 0 & \tau \\ 0 & -\tau & 0 \end{array} \right] \left[\begin{array}{l} \mathbf{T}^w \\ \mathbf{N}^w \\ \mathbf{B}^w \end{array} \right], \quad (2.1)$$

and

$$g = \|\gamma'\|, \quad \mathbf{t} = \frac{\gamma'}{g}, \quad \mathbf{n} = \mathbf{t}^\perp, \quad \kappa = \frac{\mathbf{t}' \cdot \mathbf{n}}{g}, \quad \dot{\kappa} = \frac{\kappa'}{g}, \quad (2.2)$$

where prime “'” denotes differentiation with respect to an arbitrary spatial parameter (S or s). We use dot “.” to denote differentiation with respect to arc-length (\tilde{S} or \tilde{s}) only when an entity clearly belongs to either a space or an image curve. The matrix equations on the right of (2.1) are the Frenet equations. Note that both the curvature derivatives \dot{K} and $\dot{\kappa}$ are intrinsic quantities.

2.2 Perspective Projection

The projection of a 3D space curve Γ into a 2D image curve γ is illustrated by Figure 2(a), where the world coordinate system is centered at O with basis vectors $\{\mathbf{e}_1^w, \mathbf{e}_2^w, \mathbf{e}_3^w\}$. The *camera coordinate system* is centered at \mathbf{c} with basis vectors $\{\mathbf{e}_1, \mathbf{e}_2, \mathbf{e}_3\}$. A generic way of referring to individual coordinates is by means of the specific subscripts x, y and z attached to a symbol, *i.e.*, $\mathbf{v} = [v_x, v_y, v_z]^\top$ for any vector \mathbf{v} ; other subscripts denote partial differentiation. When describing coordinates in the camera coordinate system we drop the w superscript, *e.g.*, Γ versus Γ^w , which are related by

$$\Gamma = \mathcal{R}(\Gamma^w - \mathbf{c}) = \mathcal{R}\Gamma^w + \mathcal{T}, \quad (2.3)$$

where \mathcal{R} is a rotation and $\mathcal{T} = -\mathcal{R}\mathbf{c}$ denotes the world coordinate origin in the camera coordinate system.

The projection of a 3D point $\Gamma = [x, y, z]^\top$ onto the image plane at $z = 1$ is the point $\gamma = [\xi, \eta, 1]^\top$ related by

$$\Gamma = \rho\gamma \quad \text{or} \quad [x, y, z]^\top = [\rho\xi, \rho\eta, \rho]^\top, \quad (2.4)$$

where we say that γ is in normalized image coordinates (focal distance is normalized to 1), and the depth is $\rho = z = \mathbf{e}_3^\top \Gamma$ from the third coordinate equation. Observe that image points are treated as 3D points with $z = 1$. Thus, we can write

$$\gamma = \frac{\Gamma}{\rho}. \quad (2.5)$$

We note that $\mathbf{e}_3^\top \gamma^{(i)} = 0$ and $\mathbf{e}_3^\top \Gamma^{(i)} = \rho^{(i)}$, where $\gamma^{(i)}$ is the i^{th} derivative of γ with respect to an arbitrary parameter, for any positive integer i . Specifically,

$$\rho = z, \quad \rho' = GT_z, \quad \rho'' = G'T_z + G^2KN_z. \quad (2.6)$$

It is interesting to note that at near/far points of the curve, *i.e.*, $\rho' = 0$, $T_z = 0$.

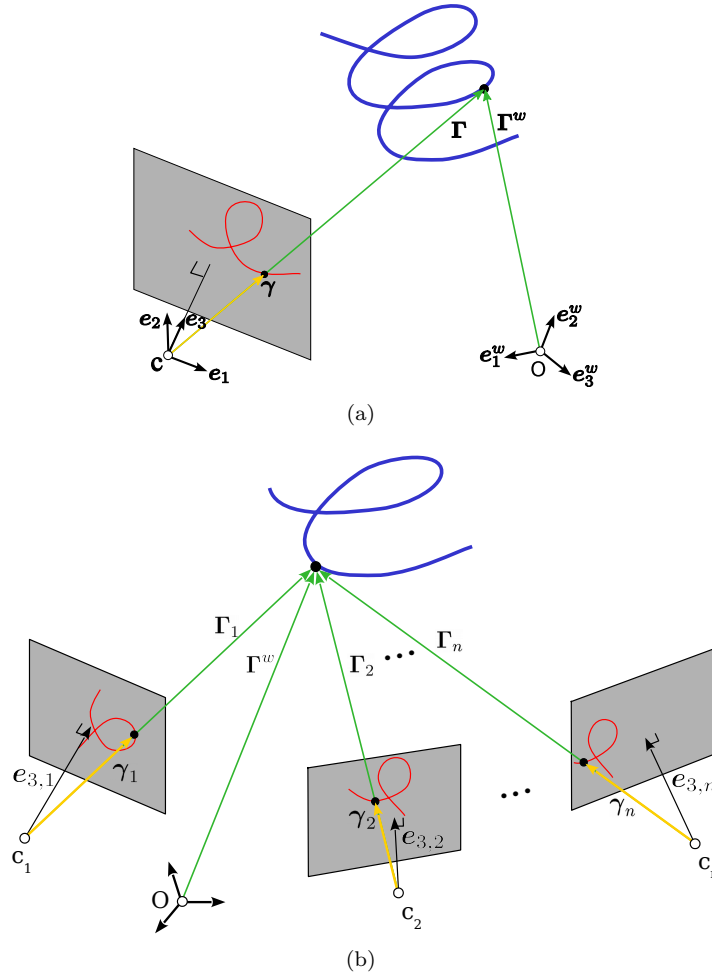


Fig. 2: The perspective projection of a space curve in (a) one view, and (b) n views.

In practice, normalized image coordinates $\gamma = [\xi, \eta, 1]^\top$ are described in terms of image pixel coordinates $\gamma_{im} = [x_{im}, y_{im}, 1]^\top$ through the intrinsic parameter matrix \mathcal{K}_{im} according to

$$\gamma_{im} = \mathcal{K}_{im}\gamma, \quad \mathcal{K}_{im} = \begin{bmatrix} \alpha_\xi & \sigma & \xi_o \\ 0 & \alpha_\eta & \eta_o \\ 0 & 0 & 1 \end{bmatrix}, \quad (2.7)$$

where as usual ξ_o and η_o are the principal points, σ is skew, and α_ξ and α_η are given by the focal length divided by the width and height of a pixel in world units, respectively.

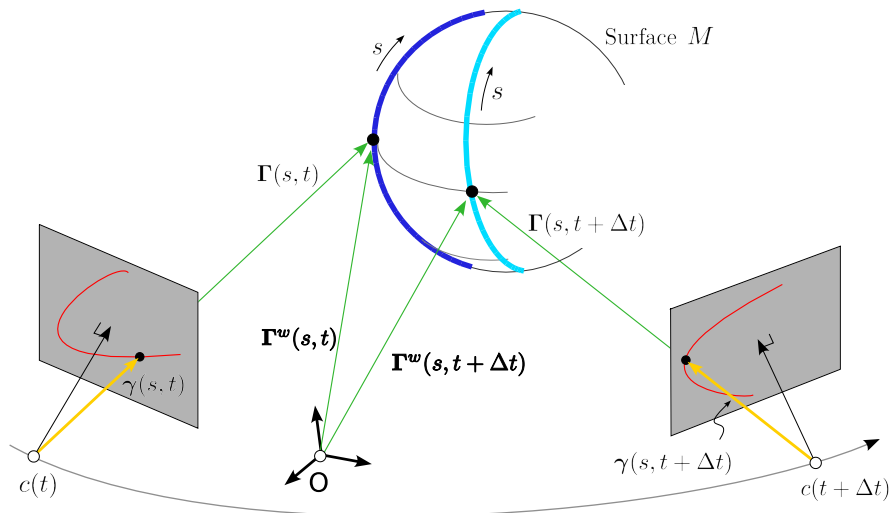


Fig. 3: Multiview formulation of continuous camera motion and a possibly moving contour.

2.3 Discrete and Continuous Sets of Views

Two scenarios are considered. The first scenario consists of a *discrete set of views* where a set of n pinhole cameras observe a scene as shown in Figure 2(b), with the last subscript in the symbols identifying the camera, e.g., γ_i denotes an image point in the i^{th} camera, and $\mathbf{e}_{3,i}$ denotes \mathbf{e}_3 in the i^{th} view. The second scenario consists of a *continuous set of views* from a continuously moving camera observing a space curve which may itself be moving, $\mathbf{I}^w(S, t) = [x^w(S, t), y^w(S, t), z^w(S, t)]^\top$, where S is the parameter along the curve and t is time, described in the camera coordinate system associated with time t as $\mathbf{I}(S, t) = [x(S, t), y(S, t), z(S, t)]^\top$, Figure 3. For simplicity, we often omit the parameters S or t . Let the camera position over time (*camera orbit*) be described by the space curve $\mathbf{c}(t)$ and the camera orientation by a rotation matrix $\mathbf{R}(t)$. For simplicity, and without loss of generality, we take the camera coordinate system at $t = 0$ to be the world coordinate system, i.e., $\mathbf{c}(0) = 0$, $\mathcal{T}(0) = 0$, and $\mathbf{R}(0) = I$, where I is the identity matrix. Also, a stationary point can be modeled in this notation by making $\mathbf{I}^w(t) = \mathbf{I}^w(0) = \mathbf{I}_0$.

A differential camera motion model using time derivatives of $\mathbf{R}(t)$ and $\mathcal{T}(t)$ can be used to relate frames in a small time interval. Since $\mathbf{R}\mathbf{R}^\top = I$,

$$\frac{d\mathbf{R}}{dt}\mathbf{R}^\top + \mathbf{R}\frac{d\mathbf{R}^\top}{dt} = 0, \quad (2.8)$$

which implies that $\mathbf{\Omega}_\times \doteq \frac{d\mathbf{R}}{dt}\mathbf{R}^\top$ is a skew-symmetric matrix, explicitly written as

$$\mathbf{\Omega}_\times = \begin{bmatrix} 0 & -\Omega_z & \Omega_y \\ \Omega_z & 0 & -\Omega_x \\ -\Omega_y & \Omega_x & 0 \end{bmatrix}, \quad (2.9)$$

Symbol	Description	Symbol	Description
Γ^w	3D point in the world coordinate system	\mathbf{t}	Image curve tangent $\mathbf{t} = \boldsymbol{\gamma}'/g$
Γ	3D point in the camera coord. syst. $\mathbf{r} = \mathcal{R}\Gamma^w + \boldsymbol{\tau}$	\mathbf{n}	Image curve normal $\mathbf{n} = \mathbf{t}^\perp$
\mathcal{R}	Rotation matrix: world to camera coordinates	κ	Curvature of the image curve $g\kappa\mathbf{n} = \mathbf{t}'$
$\boldsymbol{\tau}$	Translation vector: world to camera coord. $\boldsymbol{\tau} = -R\mathbf{c}$	S, \bar{S}	Space curve arbitrary parameter & arclength, resp.
\mathbf{c}	The camera center	G	Space curve speed of parametrization $G = \ \Gamma'\ $
Ω_\times	$\frac{d\mathcal{R}}{dt} = \Omega_\times \mathcal{R}$	\mathbf{T}, \mathbf{T}^w	Space curve tangent camera & world coord., resp.
$\boldsymbol{\Omega}$	Vector form of the 3 entries of Ω_\times	\mathbf{N}, \mathbf{N}^w	Space curve normal: camera & world coord., resp.
\mathbf{V}	$\mathbf{V} = \frac{d\boldsymbol{\tau}}{dt} = \Omega_\times \boldsymbol{\tau} - \mathcal{R}\mathbf{c}_t$, also $\mathbf{V} = [V_x, V_y, V_z]^\top$	\mathbf{B}, \mathbf{B}^w	Space curve binormal: camera & world coord., resp.
ρ	Depth of image point $\Gamma = \rho\boldsymbol{\gamma}$	$\mathbf{e}_1, \mathbf{e}_2, \mathbf{e}_3$	Basis vectors of the camera coordinate system
$\boldsymbol{\gamma}$	2D point in normalized image coordinates	$\mathbf{e}_1^w, \mathbf{e}_2^w, \mathbf{e}_3^w$	Basis vectors of the world coordinate system
$\boldsymbol{\gamma}_{im}$	2D point in pixel image coordinates	'	Diff. with resp. to S or s , depending on context
s, \bar{s}	Image curve arbitrary parameter & arclength, resp.	'	Diff. with resp. to arclength \bar{S} or \bar{s}
g	Image curve speed of parametrization $g = \ \boldsymbol{\gamma}'\ $	θ	The angle $\angle(\mathbf{T}, \boldsymbol{\gamma})$
(u, v)	Image velocities $\boldsymbol{\gamma}_t = [u, v, 0]^\top$		

Table 1: Notation.

so that $\frac{d\mathcal{R}}{dt} = \Omega_\times \mathcal{R}$. Denote $\boldsymbol{\Omega} = [\Omega_x, \Omega_y, \Omega_z]^\top$ as a vector form characterization of Ω_\times . Similarly, the second-derivative of $\mathcal{R}(t)$ is represented by only three additional numbers $\frac{d\Omega_\times}{dt}$, so that

$$\frac{d^2\mathcal{R}}{dt^2} = \frac{d\Omega_\times}{dt} \mathcal{R} + \Omega_\times \frac{d\mathcal{R}}{dt} = \frac{d\Omega_\times}{dt} \mathcal{R} + \Omega_\times^2 \mathcal{R}. \quad (2.10)$$

Thus, a second-order Taylor approximation of the camera rotation matrix using $R(0) = I$ is

$$\mathcal{R}(t) \approx I + \Omega_\times(0)t + \frac{1}{2} \left[\frac{d\Omega_\times}{dt}(0) + \Omega_\times^2(0) \right] t^2. \quad (2.11)$$

Similarly, the camera translation can be described by a differential model

$$\mathbf{V}(t) \doteq \frac{d\boldsymbol{\tau}}{dt}(t) = -\Omega_\times(t)\mathcal{R}(t)\mathbf{c}(t) - \mathcal{R}(t)\frac{d\mathbf{c}}{dt}(t), \quad \mathbf{V}(0) = -\frac{d\mathbf{c}}{dt}(0), \quad (2.12)$$

and

$$\frac{d\mathbf{V}}{dt}(t) = \frac{d^2\boldsymbol{\tau}}{dt^2}(t) = -\frac{d^2\mathcal{R}}{dt^2}(t)\mathbf{c}(t) - 2\frac{d\mathcal{R}}{dt}(t)\frac{d\mathbf{c}}{dt}(t) - \mathcal{R}(t)\frac{d^2\mathbf{c}}{dt^2}(t), \quad (2.13)$$

which at $t = 0$ gives $\frac{d\mathbf{V}}{dt}(0) = -2\Omega_\times(0)\frac{d\mathbf{c}}{dt}(0) - \frac{d^2\mathbf{c}}{dt^2}(0)$.

The choice of whether to adopt the Taylor approximation of $\mathbf{c}(t)$ or $\boldsymbol{\tau}(t)$ as primary is entirely dependent in which domain the higher derivatives are expected to diminish, giving

$$\boldsymbol{\tau}(t) \approx \mathbf{V}(0)t + \frac{1}{2} \mathbf{V}_t(0) t^2, \quad \mathbf{c}(t) \approx -\mathbf{V}(0)t + \frac{1}{2} [-\mathbf{V}_t(0) + 2\Omega_\times(0)\mathbf{V}(0)] t^2. \quad (2.14)$$

2.4 Relating World and Camera-Centric Derivatives.

Proposition 1 *The velocity of a 3D point $\Gamma(t)$ in camera coordinates, $\Gamma_t(t)$, is related to its velocity in the world coordinates $\Gamma_t^w(t)$ by*

$$\begin{cases} \Gamma_t = \Omega_{\times} \mathcal{R} \Gamma^w + \mathcal{R} \Gamma_t^w + \mathbf{V} = \Omega_{\times} \Gamma + \mathcal{R} \Gamma_t^w - \mathcal{R} \mathbf{c}_t, & (2.15) \end{cases}$$

$$\begin{cases} \Gamma_t = \Omega_{\times} \mathcal{R} \Gamma_0 + \mathbf{V} = \Omega_{\times} \Gamma - \mathcal{R} \mathbf{c}_t, \quad \text{for a fixed point, } \Gamma^w = \Gamma_0. & (2.16) \end{cases}$$

Proof Differentiating Equation 2.3 with respect to time,

$$\Gamma_t = \mathcal{R}_t \Gamma^w + \mathcal{R} \Gamma_t^w + \mathcal{T}_t \quad (2.17)$$

$$= \Omega_{\times} \mathcal{R} \Gamma^w + \mathcal{R} \Gamma_t^w + \mathbf{V} \quad (2.18)$$

$$= \Omega_{\times} (\Gamma - \mathcal{T}) + \mathcal{R} \Gamma_t^w + \mathbf{V} \quad (2.19)$$

$$= \Omega_{\times} \Gamma + \mathcal{R} \Gamma_t^w + \mathbf{V} - \Omega_{\times} \mathcal{T}. \quad (2.20)$$

The result follows from using $\mathcal{T} = -\mathcal{R} \mathbf{c}$,

$$\mathbf{V} = \mathcal{T}_t = -\mathcal{R}_t \mathbf{c} - \mathcal{R} \mathbf{c}_t = -\Omega_{\times} \mathcal{R} \mathbf{c} - \mathcal{R} \mathbf{c}_t = \Omega_{\times} \mathcal{T} - \mathcal{R} \mathbf{c}_t. \quad (2.21)$$

2.5 Stationary and Non-Stationary Contours

It is important to differentiate between image contours arising from a space curve that is changing at most with a rigid transform (stationary contours), *e.g.*, reflectance contours and sharp ridges, and image curves arising from deforming space curves (non-stationary contours), *e.g.*, occluding contours, the *contour generators* projecting to *apparent contours*. Stationary contours are characterized by $\Gamma_t^w = 0$ while for occluding contours the viewing direction $\Gamma(S, t)$ is tangent to the surface \mathcal{M} with surface normal \mathbf{N} ($\mathbf{N}^w = \mathcal{R}^{\top} \mathbf{N}$)

$$\Gamma^{\top} \mathbf{N} = 0, \quad \text{or} \quad (\Gamma^w - \mathbf{c})^{\top} \mathbf{N}^w = 0. \quad (2.22)$$

For the image curve $\gamma(s, t)$ arising from the occluding contour, Figure 3, the normal \mathbf{N} to \mathcal{M} at an occluding contour (Cipolla and Giblin 1999) can be consistently taken as $\mathbf{N} = \frac{\gamma \times t}{\|\gamma \times t\|}$.

Unless otherwise stated, we assume that the parametrization $\Gamma^w(S, t)$ of \mathcal{M} is regular for occluding contours, so that $\Gamma_S^w(S, t)$ and $\Gamma_t^w(S, t)$ form the tangent plane to \mathcal{M} at $\Gamma^w(S, t)$, and t can be seen as a spatial parameter (Giblin and Weiss 1995). The correlation of the parametrization S of Γ at time t to that of nearby times is captured by $\Gamma_t^w(S, t)$, which is orthogonal to \mathbf{N}^w (since \mathbf{N}^w is orthogonal to the tangent plane), but is otherwise arbitrary as a one dimensional choice. It is common to require that $\Gamma_t^w(S, t)$ lay on the (infinitesimal) epipolar plane, spanned by $\Gamma^w(S, t)$, $\mathbf{c}(t)$, and $\mathbf{c}_t(t)$, referred to as the *epipolar parametrization* (Cipolla and Giblin 1999; Giblin and Weiss 1995),

$$\Gamma_t^w \times (\Gamma^w - \mathbf{c}) = 0, \quad \text{or} \quad \Gamma_t^w = \lambda(\Gamma^w - \mathbf{c}) \text{ for some } \lambda. \quad (2.23)$$

3 Projecting Differential Geometry Onto a Single View

This section relates the intrinsic differential-geometric attributes of the space curve and those of its perspective image curves. Specifically, the derivatives \mathbf{I}' , \mathbf{I}'' , and \mathbf{I}''' are first expressed in terms of the differential geometry of Γ , namely $\{\mathbf{T}, \mathbf{N}, \mathbf{B}, K, \dot{K}, \tau\}$, and second, they are expressed in terms of the differential geometry of γ , namely $\{\mathbf{t}, \mathbf{n}, \kappa, \dot{\kappa}\}$ using $\mathbf{I} = \rho\gamma$. Note that \dot{K} and $\dot{\kappa}$ are both intrinsic quantities. In equating these two expressions, we relate $\{\mathbf{T}, \mathbf{N}, \mathbf{B}, K, \dot{K}, \tau\}$ to $\{\mathbf{t}, \mathbf{n}, \kappa, \dot{\kappa}\}$. Our purpose is to eliminate the dependence on the parametrizations (g, G) , and depth ρ , *i.e.*, final expressions do not contain these unknowns nor their derivatives (g, g', g'') , (G, G', G'') , or unknown depth and its derivatives $(\rho, \rho', \rho'', \rho''')$. Intrinsic camera parameters are dealt with in Section 3.1.

Proposition 2 $\{\mathbf{T}, \mathbf{N}, \mathbf{B}, K, \dot{K}, \tau, G, G', G''\}$ are related to $\{\gamma, \mathbf{t}, \mathbf{n}, \kappa, \dot{\kappa}, g, g', g'', \rho, \rho', \rho'', \rho'''\}$ by

$$\begin{cases} G\mathbf{T} = \rho'\gamma + \rho g\mathbf{t} & (3.1) \\ G'\mathbf{T} + G^2K\mathbf{N} = \rho''\gamma + (2\rho'g + \rho g')\mathbf{t} + \rho g^2\kappa\mathbf{n} & (3.2) \\ (G'' - G^3K^2)\mathbf{T} + (3GG'K + G^3\dot{K})\mathbf{N} + G^3K\tau\mathbf{B} = \\ \rho'''\gamma + [3\rho''g + 3\rho'g' + \rho(g'' - g^3\kappa^2)]\mathbf{t} + [3\rho'g^2\kappa + \rho(3gg'\kappa + g^3\dot{\kappa})]\mathbf{n}, & (3.3) \end{cases}$$

where Γ and γ are linked by a common parameter via projection $\mathbf{I} = \rho\gamma$.

Proof First, writing \mathbf{I}' , \mathbf{I}'' , and \mathbf{I}''' in the Frenet frame of \mathbf{I} as

$$\begin{cases} \mathbf{I}' = G\mathbf{T} & (3.4) \\ \mathbf{I}'' = G'\mathbf{T} + G^2K\mathbf{N} & (3.5) \\ \mathbf{I}''' = (G'' - G^3K^2)\mathbf{T} + (3GG'K + G^2K')\mathbf{N} + G^3K\tau\mathbf{B}. & (3.6) \end{cases}$$

Note that when expressed with respect to the arc-length of \mathbf{I} , *i.e.*, $G \equiv 1$, simple expressions result:

$$\begin{cases} \dot{\mathbf{I}} = \mathbf{T} & (3.7) \\ \ddot{\mathbf{I}} = K\mathbf{N} & (3.8) \\ \dddot{\mathbf{I}} = -K^2\mathbf{T} + \dot{K}\mathbf{N} + K\tau\mathbf{B}. & (3.9) \end{cases}$$

Second, differentiating $\mathbf{I} = \rho\gamma$ gives

$$\begin{cases} \mathbf{I}' = \rho'\gamma + \rho\gamma' & (3.10) \\ \mathbf{I}'' = \rho''\gamma + 2\rho'\gamma' + \rho\gamma'' & (3.11) \\ \mathbf{I}''' = \rho'''\gamma + 3\rho''\gamma' + 3\rho'\gamma'' + \rho\gamma'''. & (3.12) \end{cases}$$

This can be rewritten using expressions for the derivatives of γ , which are

$$\begin{cases} \gamma' = g\mathbf{t} & (3.13) \\ \gamma'' = g'\mathbf{t} + g^2\kappa\mathbf{n} & (3.14) \\ \gamma''' = (g'' - g^3\kappa^2)\mathbf{t} + (3gg'\kappa + g^2\kappa')\mathbf{n}. & (3.15) \end{cases}$$

Thus, \mathbf{F}' , \mathbf{F}'' , and \mathbf{F}''' can be written in terms of $\boldsymbol{\gamma}$, \mathbf{t} , \mathbf{n} , κ , $\dot{\kappa}$, g , g' , g'' , ρ , ρ' , ρ'' , ρ''' as

$$\begin{cases} \mathbf{F}' = \rho' \boldsymbol{\gamma} + \rho g \mathbf{t} & (3.16) \end{cases}$$

$$\begin{cases} \mathbf{F}'' = \rho'' \boldsymbol{\gamma} + (2\rho' g + \rho g') \mathbf{t} + \rho g^2 \kappa \mathbf{n} & (3.17) \end{cases}$$

$$\begin{cases} \mathbf{F}''' = \rho''' \boldsymbol{\gamma} + [3\rho'' g + 3\rho' g' + \rho(g'' - g^3 \kappa^2)] \mathbf{t} \\ \quad + [3\rho' g^2 \kappa + \rho(3g g' \kappa + g^3 \dot{\kappa})] \mathbf{n}. & (3.18) \end{cases}$$

Equating (3.4-3.6) and (3.16-3.18) proves the proposition.

Corollary 1 *Using the arc-length \tilde{S} of the space curve as the common parameter, i.e., when $G \equiv 1$, we have*

$$\begin{cases} \mathbf{T} = \rho' \boldsymbol{\gamma} + \rho g \mathbf{t} & (3.19) \\ KN = \rho'' \boldsymbol{\gamma} + (2\rho' g + \rho g') \mathbf{t} + \rho g^2 \kappa \mathbf{n} & (3.20) \\ -K^2 \mathbf{T} + \dot{K} \mathbf{N} + K \tau \mathbf{B} = \rho''' \boldsymbol{\gamma} + [3\rho'' g + 3\rho' g' + \rho(g'' - g^3 \kappa^2)] \mathbf{t} \\ \quad + [3\rho' g^2 \kappa + \rho(3g g' \kappa + g^3 \dot{\kappa})] \mathbf{n}. & (3.21) \end{cases}$$

First-Order Differential Geometry. We are now in a position to derive the first-order differential attributes of the image curve (g, \mathbf{t}) from that of the space curve (G, \mathbf{T}) . Note from (3.1) or (3.19) that \mathbf{T} lies on the plane spanned by \mathbf{t} and $\boldsymbol{\gamma}$, i.e., \mathbf{T} is a linear combination of these vectors. An exact relationship is expressed below.

Theorem 1 *Given the tangent \mathbf{T} at \mathbf{F} when \mathbf{T} is not aligned with $\boldsymbol{\gamma}$, then the corresponding tangent \mathbf{t} and normal \mathbf{n} at $\boldsymbol{\gamma}$ are determined by*

$$\mathbf{t} = \frac{\mathbf{T} - T_z \boldsymbol{\gamma}}{\|\mathbf{T} - T_z \boldsymbol{\gamma}\|}, \quad \mathbf{n} = \mathbf{t}^\perp \doteq \mathbf{t} \times \mathbf{e}_3. \quad (3.22)$$

Proof Equation 3.1 states that \mathbf{T} , \mathbf{t} , and $\boldsymbol{\gamma}$ are coplanar. Taking the dot product with \mathbf{e}_3 and using $\mathbf{e}_3^\top \boldsymbol{\gamma} = 1$, $\mathbf{e}_3^\top \mathbf{t} = 0$, and $\rho' = GT_z$ (Equation 2.6), isolate \mathbf{t} in the original equation as

$$\mathbf{t} = \frac{1}{\rho g} [G\mathbf{T} - \rho' \boldsymbol{\gamma}] = \frac{G}{\rho g} [\mathbf{T} - T_z \boldsymbol{\gamma}] \quad (3.23)$$

and the result follows by normalizing. The formula for the normal comes from the fact that it lies in the image plane, therefore being orthogonal to both \mathbf{t} and \mathbf{e}_3 .

Observe that the depth scale factor ρ is not needed to find \mathbf{t} from \mathbf{T} . Moreover, when $\boldsymbol{\gamma}$ and \mathbf{T} are aligned for a point on $\boldsymbol{\gamma}$, Equation 3.23 still holds, but implies that $g = 0$ and \mathbf{t} is undefined, i.e., that the image curve will have stationary points and possibly corners or cusps. Stationary points are in principle not detectable from the trace of $\boldsymbol{\gamma}$ alone, but by the assumption of general position these do not concern us.

A crucial quantity in relating differential geometry along the space curve to that of the projected image curve is the *ratio of speeds of parametrizations* $\frac{g}{G}(s)$. The following theorem derives the key result that this quantity is *intrinsic* in that it does not depend on the parametrization of Γ or of $\boldsymbol{\gamma}$, thus allowing a relationship between the differential geometry of the space and image curves.

Theorem 2 *The ratio of speeds of the projected 2D curve g and of the 3D curve G at corresponding points is an intrinsic quantity given by*

$$\frac{g}{G} = \frac{\|\mathbf{T} - T_z \boldsymbol{\gamma}\|}{z} \quad \text{or} \quad g = \frac{\|G\mathbf{T} - \rho' \boldsymbol{\gamma}\|}{\rho}, \quad (3.24)$$

i.e., it does not depend on the parametrization of \mathbf{T} or of $\boldsymbol{\gamma}$.

Proof Follows from a dot product of Equation 3.23 with \mathbf{t} and dividing by $\rho = z$.

Second-Order Differential Geometry. The curvature of an image curve can be derived from the curvature of the space curve, as shown by the next theorem.

Theorem 3 *The curvature κ of a projected image curve is given by*

$$\kappa = \left[\frac{\mathbf{N} - N_z \boldsymbol{\gamma}}{\rho g^2} \cdot \mathbf{n} \right] K, \quad \text{when } G \equiv 1, \quad \text{or} \quad \kappa = \left(\frac{G}{g} \right)^2 \left[\frac{\mathbf{N}^\top (\boldsymbol{\gamma} \times \mathbf{t})}{\rho} \right] K, \quad (3.25)$$

where g and $\frac{G}{g}$ are given by Equation 3.24, and $\rho = \mathbf{e}_3^\top \mathbf{T}$. The tangential acceleration of a projected curve with respect to the arc length of the space curve is given by

$$\frac{dg}{d\tilde{S}} = \frac{[\mathbf{N} - N_z \boldsymbol{\gamma}]^\top \mathbf{t} K}{\rho} - 2g \frac{T_z}{\rho}, \quad \text{or} \quad \frac{dg}{d\tilde{S}} = -\frac{K \mathbf{N}^\top (\boldsymbol{\gamma} \times \mathbf{n})}{\rho} - 2g \frac{T_z}{\rho}. \quad (3.26)$$

Proof Using Equation 2.6 in Equation 3.2 leads to

$$G' \mathbf{T} + G^2 K \mathbf{N} = (G' T_z + G^2 K N_z) \boldsymbol{\gamma} + 2G T_z g \mathbf{t} + \rho g' \mathbf{t} + \rho g^2 \kappa \mathbf{n}. \quad (3.27)$$

First, in the case of $G \equiv 1$ curvature κ can be isolated by taking the dot product of the last equation with \mathbf{n} which gives the curvature projection formula (3.25). By instead taking the dot product with $\boldsymbol{\gamma} \times \mathbf{t}$ we arrive at the alternative formula, since the only remaining terms are those containing \mathbf{N} or \mathbf{n} ,

$$G^2 K \mathbf{N}^\top (\boldsymbol{\gamma} \times \mathbf{t}) = \rho g^2 \kappa \mathbf{n}^\top (\boldsymbol{\gamma} \times \mathbf{t}). \quad (3.28)$$

Isolating κ and using $\mathbf{n}^\top (\boldsymbol{\gamma} \times \mathbf{t}) = \boldsymbol{\gamma}^\top (\mathbf{t} \times \mathbf{n}) = \boldsymbol{\gamma}^\top \mathbf{e}_3 = 1$ gives the desired equation. Second, the term g' can be isolated by taking the dot product with \mathbf{t} or with $\boldsymbol{\gamma} \times \mathbf{n}$, giving the first and second formulas, respectively, noting that $\mathbf{t}^\top (\boldsymbol{\gamma} \times \mathbf{n}) = -1$.

Note that formulas for the projection of 3D tangent and curvatures onto 2D tangent and geodesic curvature appear in (Cipolla and Zisserman 1992) and (Cipolla and Giblin 1999, pp. 73–75), but an actual image curvature was not determined there. That the curvature of the space curve is related to the curvature of the projected curve was derived in previous work (Li and Zucker 2003; Robert and Faugeras 1991), but our proof is much simpler and more direct. Moreover, our proof methodology generalizes to relating higher order derivatives such as curvature derivative and torsion, as shown below.

Theorem 4 *The curvature derivative of a projected image curve $\boldsymbol{\gamma}$ is derived from the local third-order differential geometry of the space curve as follows*

$$\dot{\kappa} = \frac{[\dot{K} \mathbf{N} + K \boldsymbol{\tau} \mathbf{B}]^\top (\boldsymbol{\gamma} \times \mathbf{t})}{\rho g^3} - 3\kappa \left(\frac{T_z}{\rho g} + \frac{g'}{g^2} \right), \quad (3.29)$$

assuming $G \equiv 1$.

Proof Taking the scalar product of Equation 3.21 with $\boldsymbol{\gamma} \times \mathbf{t}$, and using $\mathbf{T}^\top(\boldsymbol{\gamma} \times \mathbf{t}) = 0$ and $\mathbf{n}^\top(\boldsymbol{\gamma} \times \mathbf{t}) = \boldsymbol{\gamma}^\top(\mathbf{t} \times \mathbf{n}) = \boldsymbol{\gamma}^\top \mathbf{e}_3 = 1$,

$$[\dot{K}\mathbf{N} + K\tau\mathbf{B}]^\top(\boldsymbol{\gamma} \times \mathbf{t}) = 3\rho'g^2\kappa + \rho(3gg'\kappa + g^3\dot{\kappa}), \quad (3.30)$$

which using $\rho' = T_z$ gives

$$3T_z g^2 \kappa + \rho(3gg'\kappa + g^3\dot{\kappa}) = [\dot{K}\mathbf{N} + K\tau\mathbf{B}]^\top(\boldsymbol{\gamma} \times \mathbf{t}). \quad (3.31)$$

Isolating $\dot{\kappa}$ gives the desired result. Since both g and g' are available from Equations 3.24 and 3.26, the theorem follows.

3.1 Intrinsic Camera Parameters and Differential Geometry

This section derives the relationship between the intrinsic differential geometry $\{\mathbf{t}, \mathbf{n}, \kappa, \dot{\kappa}\}$ of the curve in normalized image coordinates to those in image pixel coordinates, $\{\mathbf{t}_{im}, \mathbf{n}_{im}, \kappa_{im}, \dot{\kappa}_{im}\}$. Using the intrinsic parameter matrix \mathcal{K}_{im} relating $\boldsymbol{\gamma}_{im} = \mathcal{K}_{im}\boldsymbol{\gamma}$, by the linear Equation 2.7.

Theorem 5 *The intrinsic quantities $\{\mathbf{t}, \mathbf{n}, \kappa, \dot{\kappa}\}$ and $\{\mathbf{t}_{im}, \mathbf{n}_{im}, \kappa_{im}, \dot{\kappa}_{im}\}$ under linear transformation $\boldsymbol{\gamma}_{im} = \mathcal{K}_{im}\boldsymbol{\gamma}$ are related by*

$$\begin{cases} g_{im} = \|\mathcal{K}_{im}\mathbf{t}\|, & \mathbf{t}_{im} = \frac{\mathcal{K}_{im}\mathbf{t}}{\|\mathcal{K}_{im}\mathbf{t}\|}, & \mathbf{n}_{im} = \mathbf{t}_{im} \times \mathbf{e}_3, & (3.32) \\ g'_{im} = \frac{\kappa\mathbf{t}^\top\mathcal{K}_{im}^\top\mathcal{K}_{im}\mathbf{n}}{g_{im}}, & \kappa_{im} = \frac{\mathbf{n}_{im}^\top\mathcal{K}_{im}\kappa\mathbf{n}}{g_{im}^2}, & & (3.33) \\ \dot{\kappa}_{im} = \frac{1}{g_{im}^3}\mathbf{n}_{im}^\top\mathcal{K}_{im}(-\kappa^2\mathbf{t} + \dot{\kappa}\mathbf{n}) - \frac{3g'_{im}\kappa_{im}}{g_{im}^2}. & & & (3.34) \end{cases}$$

where the speed g_{im} is relative to unit speed at $\boldsymbol{\gamma}$.

Proof Differentiating (2.7) with respect to the arc-length \tilde{s} of $\boldsymbol{\gamma}$ and using (3.13), $\boldsymbol{\gamma}'_{im} = \mathcal{K}_{im}\dot{\boldsymbol{\gamma}}$ gives

$$g_{im}\mathbf{t}_{im} = \mathcal{K}_{im}\mathbf{t}. \quad (3.35)$$

Differentiating (2.7) a second time with respect to \tilde{s} , and using Equation 3.14,

$$g'_{im}\mathbf{t}_{im} + g_{im}^2\kappa_{im}\mathbf{n}_{im} = \mathcal{K}_{im}\kappa\mathbf{n}. \quad (3.36)$$

Taking the dot product with \mathbf{t}_{im} gives the formula for g'_{im} , and taking the dot product with \mathbf{n}_{im} gives the formula for κ_{im} . Differentiating (2.7) a third time with respect to \tilde{s} , and using Equation 3.15, we have

$$(g''_{im} - g_{im}^3\kappa_{im}^2)\mathbf{t}_{im} + (3g_{im}g'_{im}\kappa_{im} + g_{im}^3\dot{\kappa}_{im})\mathbf{n}_{im} = \mathcal{K}_{im}(-\kappa^2\mathbf{t} + \dot{\kappa}\mathbf{n}). \quad (3.37)$$

Taking the dot product with \mathbf{n}_{im} ,

$$3g_{im}g'_{im}\kappa_{im} + g_{im}^3\dot{\kappa}_{im} = \mathbf{n}_{im}^\top\mathcal{K}_{im}(-\kappa^2\mathbf{t} + \dot{\kappa}\mathbf{n}), \quad (3.38)$$

and isolating $\dot{\kappa}_{im}$, the last result follows.

The above theorem can also be used in its inverse form from $\boldsymbol{\gamma}_{im}$ to $\boldsymbol{\gamma}$ by substituting \mathcal{K}_{im} for \mathcal{K}_{im}^{-1} , and trivially exchanging the sub-indices. Moreover, the theorem is generally valid for relating differential geometry under any linear transformation in place of \mathcal{K}_{im} .

4 Reconstructing Differential Geometry from Multiple Views

In the previous section, we derived the differential geometry of a projected curve from a space curve. In this section, we derive the differential geometry of a space curve Γ from that of its projected image curves in multiple views, namely γ_i for camera i , $i = 1, \dots, N$. In order to simplify the equations, in this section *all vectors are written in the common world coordinate basis*, including γ_i . Denote $\mathbf{F}_i := \mathbf{F}^w - \mathbf{c}_i$, namely \mathbf{F}_i represents the vector from the i^{th} camera center to the 3D point \mathbf{F}^w in the world coordinate system.

The reconstruction of a point on the space curve Γ from two corresponding image curve points γ_1 and γ_2 can be obtained by equating the two expressions for \mathbf{F}^w given by Equation 2.4,

$$\begin{cases} \mathbf{F}^w - \mathbf{c}_1 = \rho_1 \gamma_1 \\ \mathbf{F}^w - \mathbf{c}_2 = \rho_2 \gamma_2 \end{cases} \implies \rho_1 \gamma_1 - \rho_2 \gamma_2 = \mathbf{c}_2 - \mathbf{c}_1. \quad (4.1)$$

Taking the dot product with γ_1 , γ_2 , and $\gamma_1 \times \gamma_2$ gives

$$\begin{cases} \rho_1 \gamma_1 \cdot \gamma_1 - \rho_2 \gamma_1 \cdot \gamma_2 = (\mathbf{c}_2 - \mathbf{c}_1) \cdot \gamma_1 \\ \rho_1 \gamma_1 \cdot \gamma_2 - \rho_2 \gamma_2 \cdot \gamma_2 = (\mathbf{c}_2 - \mathbf{c}_1) \cdot \gamma_2 \\ 0 = (\mathbf{c}_2 - \mathbf{c}_1) \cdot (\gamma_1 \times \gamma_2), \end{cases} \quad (4.2)$$

which gives

$$\begin{cases} \rho_1 = \frac{(\mathbf{c}_2 - \mathbf{c}_1) \cdot \gamma_1 (\gamma_2 \cdot \gamma_2) - (\mathbf{c}_2 - \mathbf{c}_1) \cdot \gamma_2 (\gamma_1 \cdot \gamma_2)}{(\gamma_1 \cdot \gamma_1)(\gamma_2 \cdot \gamma_2) - (\gamma_1 \cdot \gamma_2)^2} \\ \rho_2 = \frac{(\mathbf{c}_2 - \mathbf{c}_1) \cdot \gamma_1 (\gamma_1 \cdot \gamma_2) - (\mathbf{c}_2 - \mathbf{c}_1) \cdot \gamma_2 (\gamma_1 \cdot \gamma_1)}{(\gamma_1 \cdot \gamma_1)(\gamma_2 \cdot \gamma_2) - (\gamma_1 \cdot \gamma_2)^2}, \end{cases} \quad (4.3)$$

provided that $(\mathbf{c}_2 - \mathbf{c}_1) \cdot (\gamma_1 \times \gamma_2) = 0$. This is precisely the well-known fact that this system of three equations in two unknowns ρ_1 and ρ_2 can only be solved if the lines $\mathbf{c}_1 \gamma_1$ and $\mathbf{c}_2 \gamma_2$ intersect.

The crucial factor in relating the differential geometry of image curves in distinct views is the relationship between their parametrization in each view, given in the next theorem.

Proposition 3 *The ratio of parametrization speeds in two views of a space curve at corresponding points is given by*

$$\frac{g_1}{g_2} = \frac{\rho_2 \|\mathbf{T} - (\mathbf{e}_{3,1}^\top \mathbf{T}) \gamma_1\|}{\rho_1 \|\mathbf{T} - (\mathbf{e}_{3,2}^\top \mathbf{T}) \gamma_2\|}. \quad (4.4)$$

Proof Follows by dividing expressions for $\frac{g_1}{G}$ and $\frac{g_2}{G}$ from Equation 3.24.

Next, note from Equation 3.1 that the unit vector \mathbf{T} can be written as

$$\mathbf{T} = \frac{\rho'}{G} \gamma + \rho \frac{g}{G} \mathbf{t}. \quad (4.5)$$

Since \mathbf{T} is a unit vector, it can be written as

$$\mathbf{T} = \cos \theta \frac{\gamma}{\|\gamma\|} + \sin \theta \mathbf{t}, \quad \text{where } \cos \theta = \frac{\rho'}{G} \|\gamma\|, \quad \sin \theta = \rho \frac{g}{G}. \quad (4.6)$$

Note that $\rho > 0$ implies that $\sin \theta \geq 0$ or $\theta \in [0, \pi)$. Thus the reconstruction of \mathbf{T} from \mathbf{t} requires the discovery of the additional parameter θ which can be provided from tangents at two corresponding points, as stated in the next result.

Theorem 6 Two tangent vectors at a corresponding pair of points, namely \mathbf{t}_1 at γ_1 and \mathbf{t}_2 at γ_2 , reconstruct the corresponding space tangent \mathbf{T} at Γ as

$$\mathbf{T} = \cos \theta_1 \frac{\gamma_1}{\|\gamma_1\|} + \sin \theta_1 \mathbf{t}_1 = \cos \theta_2 \frac{\gamma_2}{\|\gamma_2\|} + \sin \theta_2 \mathbf{t}_2, \quad (4.7)$$

and

$$\begin{aligned} \rho_1 g_1 = \sin \theta_1 G, & \quad \rho'_1 \|\gamma_1\| = \cos \theta_1 G, & \quad \frac{\rho'_1}{\rho_1 g_1} = -\frac{\mathbf{t}_1 \cdot (\gamma_2 \times \mathbf{t}_2)}{\gamma_1 \cdot (\gamma_2 \times \mathbf{t}_2)} \\ \rho_2 g_2 = \sin \theta_2 G, & \quad \rho'_2 \|\gamma_2\| = \cos \theta_2 G, & \quad \frac{\rho'_2}{\rho_2 g_2} = -\frac{\mathbf{t}_2 \cdot (\gamma_1 \times \mathbf{t}_1)}{\gamma_2 \cdot (\gamma_1 \times \mathbf{t}_1)}, \end{aligned} \quad (4.8)$$

where

$$\begin{aligned} \tan \theta_1 &= -\frac{1}{\|\gamma_1\|} \frac{\gamma_1 \cdot (\gamma_2 \times \mathbf{t}_2)}{\mathbf{t}_1 \cdot (\gamma_2 \times \mathbf{t}_2)}, & \quad \theta_1 \in [0, \pi) \\ \tan \theta_2 &= -\frac{1}{\|\gamma_2\|} \frac{\gamma_2 \cdot (\gamma_1 \times \mathbf{t}_1)}{\mathbf{t}_2 \cdot (\gamma_1 \times \mathbf{t}_1)}, & \quad \theta_2 \in [0, \pi). \end{aligned} \quad (4.9)$$

Proof Equating the two expressions for \mathbf{T} from Equation 4.6, one for each view, gives Equation 4.7. Solving for θ_1 by taking the dot product with $\gamma_2 \times \mathbf{t}_2$ gives

$$\cos \theta_1 \frac{\gamma_1}{\|\gamma_1\|} \cdot (\gamma_2 \times \mathbf{t}_2) + \sin \theta_1 \mathbf{t}_1 \cdot (\gamma_2 \times \mathbf{t}_2) = 0, \quad (4.10)$$

which leads to Equation 4.9 and similarly for θ_2 . Equation 4.8 follows from equating (4.10) and (4.5), then taking dot products with $\gamma_2 \times \mathbf{t}_2$.

Remark: Since \mathbf{T} is orthogonal to both $\gamma_1 \times \mathbf{t}_1$, and $\gamma_2 \times \mathbf{t}_2$ we have

$$\varepsilon \mathbf{T} = \frac{(\mathbf{t}_1 \times \gamma_1) \times (\mathbf{t}_2 \times \gamma_2)}{\|(\mathbf{t}_1 \times \gamma_1) \times (\mathbf{t}_2 \times \gamma_2)\|} \quad \varepsilon = \pm 1, \quad (4.11)$$

where ε is determined from

$$\begin{cases} \varepsilon [\mathbf{T} - (\mathbf{T} \cdot \mathbf{e}_{3,1}) \gamma_1] \cdot \mathbf{t}_1 > 0 \\ \varepsilon [\mathbf{T} - (\mathbf{T} \cdot \mathbf{e}_{3,2}) \gamma_2] \cdot \mathbf{t}_2 > 0. \end{cases} \quad (4.12)$$

Remark: This theorem implies that *any* two tangents at corresponding points can be consistent with at least one space tangent. Furthermore, the discovery of \mathbf{T} does not require the *a priori* solution of ρ_1 or ρ_2 .

Remark: An analogous tangent reconstruction expression under continuous motion may be derived, see (Faugeras and Papadopoulou 1993).

Theorem 7 The normal vector \mathbf{N} and curvature K of a point on a space curve Γ with point-tangent-curvature at projections in two views $(\gamma_1, \mathbf{t}_1, \kappa_1)$ and $(\gamma_2, \mathbf{t}_2, \kappa_2)$ are given by solving the system in the vector $\mathbf{N}K$

$$\begin{cases} G^2(\gamma_1 \times \mathbf{t}_1)^\top \mathbf{N}K = \rho_1 g_1^2 \kappa_1 \\ G^2(\gamma_2 \times \mathbf{t}_2)^\top \mathbf{N}K = \rho_2 g_2^2 \kappa_2 \\ \mathbf{T}^\top \mathbf{N}K = 0, \end{cases} \quad (4.13)$$

where \mathbf{T} is given by Equation 4.5, ρ_1 and ρ_2 by Equation 4.3, and g_1 and g_2 by Equation 3.24.

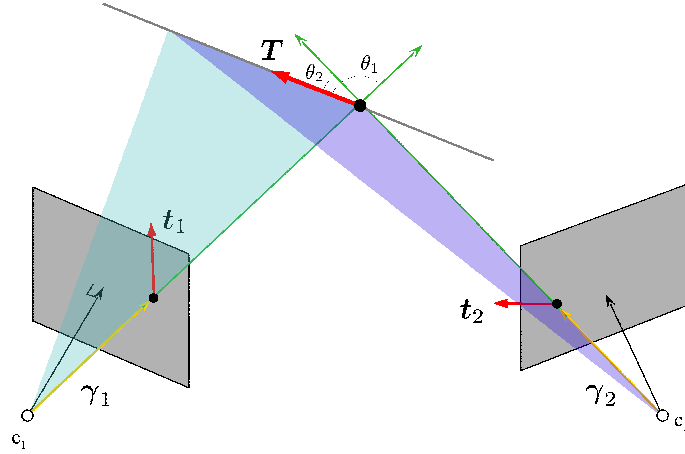


Fig. 4: 3D Tangent reconstruction from two views as the intersection of two planes.

Proof Taking the dot product of (3.27) with $\gamma \times t$, for each view, we arrive at the first two equations. The third equation imposes the solution \mathbf{NK} to be normal to \mathbf{T} .

An analogous curvature reconstruction expression under continuous motion can be derived, see (Cipolla 1991). Theorem 7 is a variant form of a known result (Robert and Faugeras 1991; Li and Zucker 2003, 2006), using the proposed unified formulation which enables a more condensed and generalizable proof for the practical case of planar images. The next theorem leverages this effective theoretical framework to achieve the reconstruction of the torsion and curvature derivative of a space curve from two image curves, which is the central novel result of the present work.

Theorem 8 *The torsion and curvature derivative at a point of a space curve can be obtained from up to third order differential geometry $\{\kappa, \dot{\kappa}\}$ at a pair of corresponding points in two views by solving for an unknown vector \mathbf{Z} in the system*

$$\begin{cases} (\gamma_1 \times \mathbf{t}_1)^\top \mathbf{Z} = 3g_1^2 \kappa_1 \mathbf{e}_{3,1}^\top \mathbf{T} + \rho_1 (3g_1 g_1' \kappa_1 + g_1^3 \dot{\kappa}_1) \\ (\gamma_2 \times \mathbf{t}_2)^\top \mathbf{Z} = 3g_2^2 \kappa_2 \mathbf{e}_{3,2}^\top \mathbf{T} + \rho_2 (3g_2 g_2' \kappa_2 + g_2^3 \dot{\kappa}_2) \\ \mathbf{T}^\top \mathbf{Z} = 0, \end{cases} \quad (4.14)$$

and by solving for the torsion τ and curvature derivative \dot{K} from $\mathbf{Z} = \dot{K} \mathbf{N} + K \tau \mathbf{B}$, i.e.,

$$\begin{cases} \tau = \frac{\mathbf{Z}^\top \mathbf{B}}{K} \\ \dot{K} = \mathbf{Z}^\top \mathbf{N}, \end{cases} \quad (4.15)$$

with \mathbf{T} , \mathbf{N} , \mathbf{B} , K , g_1 , g_2 , g_1' , g_2' , ρ_1 , and ρ_2 determined from previous derivations, and assuming $G \equiv 1$.

Proof Apply Equation (3.30) for two views, and let $\mathbf{Z} := \dot{K} \mathbf{N} + K \tau \mathbf{B}$ to get the first two equations of (4.14). The last equation of (4.14) constrains \mathbf{Z} to be orthogonal to \mathbf{T} .

5 Projecting Differential Geometry Under Differential Motion

The goal of this section is to relate *differential observations* in a series of images from a continuous video sequence to the *differential geometry* of the space curve. As this relationship is governed by the *differential motion* of the camera and its intrinsic parameters, we also aim to recover scene geometry and camera motion/pose from these observations and equations. An account of intrinsic camera calibration in this setting is left for future work. We explore how differential scene properties are projected onto differential image properties for points and curves, and expect future work to apply this to surfaces.

Differential models of camera motion observing a *rigid scene* were studied in (Longuet-Higgins and Prazdny 1980; Waxman and Ullman 1985; Maybank 1992; Ma et al 2004; van den Hengel 2000; Triggs 1999; Astrom and Heyden 1996; Heyden 2006; Baumela et al 2000; Dornaika and Sappa 2006; Kahl and Heyden 2001; Vieville and Faugeras 1996; van den Hengel et al 2007; Brodský et al 2000; Brodský and Fermüller 2002). These papers studied how the first and second-order motion of the image of fixed points relate to a differential camera motion model. They also envisioned recovering local 3D surface properties from the local behavior of the velocities of projected surface points in an image neighborhood. Differential models for *nonrigid curves* observed in a monocular video sequence were studied in (Faugeras and Papadopoulo 1993; Papadopoulo and Faugeras 1996; Papadopoulo 1996; Faugeras 1990), where it was established that multiple simultaneous video sequences would be needed. This led to a practical work in the reconstruction of nonrigid curves from multiview video (Carceroni and Kutulakos 1999; Carceroni 2001), exploiting temporal consistency within each video frame, as well as consistency across the two video sequences. Differential models of occluding contours were studied mainly in (Cipolla 1991; Cipolla and Blake 1992; Cipolla and Giblin 1999), relating the deformation of apparent contours under differential camera motion to scene properties such as occluding contours, and a differential-geometric model of the underlying 3D surface.

5.1 Differential Relations for a Point

Theorem 9 (*Moving 3D point*) Let $\mathbf{I}^w(t)$ be a moving point in space, projected onto a moving camera as $\gamma(t)$ with depth $\rho(t)$. Let the differential velocity and rotation of the camera be \mathbf{V} and $\mathbf{\Omega}$, respectively, and let \mathbf{V}_t and $\mathbf{\Omega}_t$ represent their derivative with respect to time t , respectively. Then, the depth gradient and second derivative at $t = 0$ are

$$\begin{cases} \rho_t = \rho \mathbf{e}_3^\top (\mathbf{\Omega}_\times \gamma + \frac{1}{\rho} \mathbf{I}_t^w + \frac{1}{\rho} \mathbf{V}) \\ \rho_{tt} = \rho \mathbf{e}_3^\top (\mathbf{\Omega}_\times^2 + [\mathbf{\Omega}_t]_\times) \gamma + 2\mathbf{e}_3^\top \mathbf{\Omega}_\times \mathbf{I}_t^w + \mathbf{e}_3^\top \mathbf{I}_{tt}^w + \mathbf{e}_3^\top \mathbf{V}_t, \end{cases} \quad \text{at } t = 0 \quad (5.1)$$

$$(5.2)$$

and the velocity and acceleration of the projected point at $t = 0$ are given by

$$\begin{cases} \gamma_t = (\mathbf{\Omega}_\times \gamma - (\mathbf{e}_3^\top \mathbf{\Omega}_\times \gamma) \gamma) + \frac{1}{\rho} (\mathbf{I}_t^w - \mathbf{e}_3^\top \mathbf{I}_t^w \gamma) + \frac{1}{\rho} (\mathbf{V} - V_z \gamma) \\ \gamma_{tt} = (\mathbf{\Omega}_\times^2 + [\mathbf{\Omega}_t]_\times) \gamma + \frac{2}{\rho} \mathbf{\Omega}_\times \mathbf{I}_t^w + \frac{1}{\rho} \mathbf{I}_{tt}^w + \frac{1}{\rho} \mathbf{V}_t - \frac{2\rho_t}{\rho} \gamma_t - \frac{\rho_{tt}}{\rho} \gamma, \end{cases} \quad \text{at } t = 0 \quad (5.3)$$

$$(5.4)$$

which can be simplified as

$$\begin{aligned}
\gamma_{tt} &= (\Omega_{\times}^2 + [\Omega_t]_{\times})\gamma + \frac{2}{\rho}\Omega_{\times}\Gamma_t^w + \frac{1}{\rho}\Gamma_{tt}^w + \frac{1}{\rho}\mathbf{V}_t \\
&\quad - 2\mathbf{e}_3^{\top} \left(\Omega_{\times}\gamma + \frac{\mathbf{V}}{\rho} + \frac{\Gamma_t^w}{\rho} \right) \left(\frac{\mathbf{V}}{\rho} - \frac{V_z}{\rho}\gamma + \Omega_{\times}\gamma - (\mathbf{e}_3^{\top}\Omega_{\times}\gamma)\gamma + \frac{1}{\rho}\Gamma_t^w - \frac{\mathbf{e}_3^{\top}\Gamma_t^w}{\rho}\gamma \right) \\
&\quad - \mathbf{e}_3^{\top} \left((\Omega_{\times}^2 + [\Omega_t]_{\times})\gamma + \frac{\mathbf{V}_t}{\rho} + 2\Omega_{\times}\frac{\Gamma_t^w}{\rho} + \frac{\Gamma_{tt}^w}{\rho} \right) \gamma.
\end{aligned} \tag{5.5}$$

Proof The image velocity γ_t is dependent on the velocity Γ_t of the 3D structure in camera coordinates, which arises from both the motion of Γ^w and from the moving camera. Differentiating $\Gamma = \mathcal{R}\Gamma^w + \mathcal{T}$, we get

$$\Gamma_t = \mathcal{R}_t\Gamma^w + \mathcal{R}\Gamma_t^w + \mathcal{T}_t = \Omega_{\times}\mathcal{R}\Gamma^w + \mathcal{R}\Gamma_t^w + \mathbf{V}. \tag{5.6}$$

Differentiating $\Gamma = \rho\gamma$ we get

$$\Gamma_t = \rho\gamma_t + \rho_t\gamma. \tag{5.7}$$

Equating these two expressions leads to

$$\rho\gamma_t + \rho_t\gamma = \Omega_{\times}\mathcal{R}\Gamma^w + \mathcal{R}\Gamma_t^w + \mathbf{V} \quad \text{for arbitrary } t. \tag{5.8}$$

At $t = 0$ we have $\Gamma^w = \Gamma = \rho\gamma$, leading to

$$\rho\gamma_t + \rho_t\gamma = \rho\Omega_{\times}\gamma + \Gamma_t^w + \mathbf{V} \quad \text{for } t = 0. \tag{5.9}$$

The depth gradient ρ_t is then isolated by taking the dot product of both sides of Equation 5.9 with \mathbf{e}_3 , observing that $\mathbf{e}_3^{\top}\gamma = 1$ and $\mathbf{e}_3^{\top}\gamma_t = 0$, resulting in Equation 5.1. The expression for ρ_t is then substituted into Equation 5.9 from which γ_t can be isolated in the form of Equation 5.3.

The second order expressions γ_{tt} and ρ_{tt} require another time derivative of Equation 5.8,

$$\rho\gamma_{tt} + 2\rho_t\gamma_t + \rho_{tt}\gamma = (\Omega_{\times}^2\mathcal{R} + [\Omega_t]_{\times}\mathcal{R})\Gamma^w + \Omega_{\times}\mathcal{R}\Gamma_t^w + \mathcal{R}_t\Gamma_t^w + \mathcal{R}\Gamma_{tt}^w + \mathbf{V}_t. \tag{5.10}$$

Setting $t = 0$ we have

$$\rho\gamma_{tt} + 2\rho_t\gamma_t + \rho_{tt}\gamma = (\Omega_{\times}^2 + [\Omega_t]_{\times})\rho\gamma + 2\Omega_{\times}\Gamma_t^w + \Gamma_{tt}^w + \mathbf{V}_t. \tag{5.11}$$

Now the expression for ρ_{tt} in the theorem can be obtained by dotting with \mathbf{e}_3 , giving Equation 5.2. Isolating γ_{tt} we have

$$\gamma_{tt} = (\Omega_{\times}^2 + [\Omega_t]_{\times})\gamma + \frac{1}{\rho}(2\Omega_{\times}\Gamma_t^w + \Gamma_{tt}^w + \mathbf{V}_t - 2\rho_t\gamma_t - \rho_{tt}\gamma). \tag{5.12}$$

Substituting Equations 5.2 and 5.3 into the above, we obtain the final expression for γ_{tt} .

The Special Case of Fixed Points. The question of how the image of a fixed point moves as the camera moves was studied by Longuet-Higgins and Prazdny (Longuet-Higgins and Prazdny 1980) and later by Waxman and Ullman (Waxman and Ullman 1985), giving the velocity γ_t for a fixed point. This calculation also leads to the well-known epipolar constraint, the notion of Essential matrix (Longuet-Higgins 1981), and the *continuous epipolar constraint* (Zhuang and Haralick 1984; Maybank 1992; Kanatani 1993; Viéville and Faugeras 1995; Tian et al 1996; Brooks et al 1997;

Åström and Heyden 1998; Ponce and Genc 1998; Yi Ma 1998; Ma et al 2004; Stewénius et al 2007; Lin et al 2009; Valgaerts et al 2012; Schneevogt et al 2014). Theorem 9 in the special case of a fixed point gives interesting geometric insight into these classical results. Specifically, setting $\mathbf{I}_t^w = 0$ in first-order computations of Equations 5.1 and 5.3 results in

$$\begin{cases} \frac{\rho_t}{\rho} = \mathbf{e}_3^\top (\boldsymbol{\Omega}_\times \boldsymbol{\gamma} + \frac{\mathbf{V}}{\rho}) \\ \boldsymbol{\gamma}_t = \boldsymbol{\Omega}_\times \boldsymbol{\gamma} - (\mathbf{e}_3^\top \boldsymbol{\Omega}_\times \boldsymbol{\gamma}) \boldsymbol{\gamma} + \frac{\mathbf{V}}{\rho} - \frac{V_z}{\rho} \boldsymbol{\gamma}. \end{cases} \quad \text{at } t = 0 \quad (5.13)$$

$$\quad (5.14)$$

Essential constraint. To derive the differential epipolar constraint, eliminate ρ from Equation 5.14 by first writing out the expression in terms of ξ , η , u , and v , where $\boldsymbol{\gamma} = [\xi, \eta, 1]^\top$, and $\boldsymbol{\gamma}_t = [u, v, 0]$, and use $\mathbf{e}_3^\top \boldsymbol{\Omega}_\times \boldsymbol{\gamma} = -\Omega_y \xi + \Omega_x \eta$, giving

$$\begin{cases} u - \Omega_y \xi^2 + \Omega_x \xi \eta + \Omega_z \eta - \Omega_y = \frac{1}{\rho} (V_x - V_z \xi) \\ v + \Omega_x \eta^2 - \Omega_y \xi \eta - \Omega_z \xi + \Omega_x = \frac{1}{\rho} (V_y - V_z \eta) \end{cases} \quad (5.15)$$

and then eliminate ρ , giving

$$(u - \Omega_y \xi^2 + \Omega_x \xi \eta + \Omega_z \eta - \Omega_y) (V_y - \eta V_z) = (v + \Omega_x \eta^2 - \Omega_y \xi \eta - \Omega_z \xi + \Omega_x) (V_x - \xi V_z),$$

which is the epipolar constraint for differential motion. A more direct way of deriving the epipolar constraint equation is to eliminate ρ in Equation 5.9 with $\mathbf{I}_t^w = 0$ by taking the dot-product with the vector $\mathbf{V} \times \boldsymbol{\gamma} = \mathbf{V}_\times \boldsymbol{\gamma}$, where \mathbf{V}_\times is a skew-symmetric arrangement of \mathbf{V} , and using $\boldsymbol{\Omega}_\times^\top = -\boldsymbol{\Omega}_\times$ gives

$$\rho \boldsymbol{\gamma}_t^\top \mathbf{V}_\times \boldsymbol{\gamma} = -\rho \boldsymbol{\gamma}^\top \boldsymbol{\Omega}_\times \mathbf{V}_\times \boldsymbol{\gamma},$$

resulting in the *differential epipolar constraint*

$$\boldsymbol{\gamma}_t^\top \mathbf{V}_\times \boldsymbol{\gamma} + \boldsymbol{\gamma}^\top \boldsymbol{\Omega}_\times \mathbf{V}_\times \boldsymbol{\gamma} = 0. \quad (5.16)$$

In comparison, the widely-known essential constraint for relating two views is given by

$$\boldsymbol{\gamma}_2^\top \mathcal{T}_\times \mathcal{R} \boldsymbol{\gamma}_1 = 0, \quad (5.17)$$

where $\mathcal{T}_\times \mathcal{R}$, the essential matrix, combines the effects of translation and rotation to relate two points $\boldsymbol{\gamma}_1$ and $\boldsymbol{\gamma}_2$. In the differential case, the two matrices \mathbf{V}_\times and $\boldsymbol{\Omega}_\times \mathbf{V}_\times$ play a similar role to $\mathcal{T}_\times \mathcal{R}$ in the discrete motion case to relate a point and its velocity.

Remark 1 Observe from Equation 5.14 that $\boldsymbol{\gamma}_t$ can also be written as the sum of two components, one depending on \mathbf{V} , and the other on $\boldsymbol{\Omega}$, *i.e.*,

$$\boldsymbol{\gamma}_t = \frac{1}{\rho} A(\boldsymbol{\gamma}) \mathbf{V} + B(\boldsymbol{\gamma}) \boldsymbol{\Omega}, \quad \text{where } A(\boldsymbol{\gamma}) = \begin{bmatrix} 1 & 0 & -\xi \\ 0 & 1 & -\eta \\ 0 & 0 & 0 \end{bmatrix} \quad \text{and } B(\boldsymbol{\gamma}) = \begin{bmatrix} -\xi \eta & 1 + \xi^2 & -\eta \\ -(1 + \eta) & \xi \eta & \xi \\ 0 & 0 & 0 \end{bmatrix}. \quad (5.18)$$

That $\boldsymbol{\gamma}_t$ depends linearly on \mathbf{V} and $\boldsymbol{\Omega}$ (since A and B are only dependent on the position $\boldsymbol{\gamma}$), with ρ left in the equation, is the basis of subspace methods in structure from motion (Heeger and Jepson 1992). Observations of image velocities $\boldsymbol{\gamma}_{t,1}, \boldsymbol{\gamma}_{t,2}, \dots, \boldsymbol{\gamma}_{t,N}$ at points $\boldsymbol{\gamma}_1, \boldsymbol{\gamma}_2, \dots, \boldsymbol{\gamma}_N$ provides $2N$ linear equations in \mathbf{V} and $\boldsymbol{\Omega}$, given ρ_1, \dots, ρ_N .

5.2 Differential Relations for a Curve

Theorem 10 (*Deforming 3D curve*) Consider a deforming 3D curve $\Gamma(s, t)$ projecting to a family of 2D curves $\gamma(s, t)$ with depth $\rho(s, t)$, arising from camera motion with differential velocities of translation and rotation \mathbf{V} and $\mathbf{\Omega}$, respectively, and let \mathbf{V}_t and $\mathbf{\Omega}_t$ be their respective derivatives in time. Then, the image velocity γ_t is determined from $\left\{ \mathbf{V}, \mathbf{\Omega}, \frac{\mathbf{V}}{\rho}, \frac{\mathbf{\Omega}_t^w}{\rho}, \mathbf{t} \right\}$,

$$\gamma_t = \alpha \mathbf{t} + \beta \mathbf{n}, \text{ where } \begin{cases} \alpha = -\mathbf{\Omega} \cdot \gamma \times (\gamma \times \mathbf{n}) - \left(\frac{\mathbf{V}}{\rho} - \mathbf{\Omega}_\times \frac{\mathcal{T}}{\rho} + \mathcal{R} \frac{\mathbf{\Gamma}_t^w}{\rho} \right) \cdot \gamma \times \mathbf{n}, & (5.19) \\ \beta = \mathbf{\Omega} \cdot \gamma \times (\gamma \times \mathbf{t}) + \left(\frac{\mathbf{V}}{\rho} - \mathbf{\Omega}_\times \frac{\mathcal{T}}{\rho} + \mathcal{R} \frac{\mathbf{\Gamma}_t^w}{\rho} \right) \cdot \gamma \times \mathbf{t}. & (5.20) \end{cases}$$

Proof From Equation 2.15 and using $-\mathcal{R}\mathbf{c}_t = \mathbf{V} - \mathbf{\Omega}_\times \mathcal{T}$ from Equation 2.12,

$$\mathbf{\Gamma}_t = \mathbf{\Omega}_\times \mathbf{\Gamma} + \mathbf{V} - \mathbf{\Omega}_\times \mathcal{T} + \mathcal{R} \mathbf{\Gamma}_t^w. \quad (5.21)$$

Using $\mathbf{\Gamma} = \rho \gamma$ and $\mathbf{\Gamma}_t = \rho_t \gamma + \rho \gamma_t$,

$$\rho_t \gamma + \rho \gamma_t = \rho \mathbf{\Omega}_\times \gamma + \mathbf{V} - \mathbf{\Omega}_\times \mathcal{T} + \mathcal{R} \mathbf{\Gamma}_t^w. \quad (5.22)$$

Taking the dot product with $\gamma \times \mathbf{n}$ and $\gamma \times \mathbf{t}$,

$$\begin{cases} \rho \gamma_t \cdot (\gamma \times \mathbf{n}) = \rho (\mathbf{\Omega}_\times \gamma) \cdot (\gamma \times \mathbf{n}) + (\mathbf{V} - \mathbf{\Omega}_\times \mathcal{T}) \cdot (\gamma \times \mathbf{n}) + \mathcal{R} \mathbf{\Gamma}_t^w \cdot (\gamma \times \mathbf{n}), \\ \rho \gamma_t \cdot (\gamma \times \mathbf{t}) = \rho (\mathbf{\Omega}_\times \gamma) \cdot (\gamma \times \mathbf{t}) + (\mathbf{V} - \mathbf{\Omega}_\times \mathcal{T}) \cdot (\gamma \times \mathbf{t}) + \mathcal{R} \mathbf{\Gamma}_t^w \cdot (\gamma \times \mathbf{t}). \end{cases} \quad (5.23)$$

Now,

$$\begin{cases} \gamma_t \cdot (\gamma \times \mathbf{n}) = (\alpha \mathbf{t} + \beta \mathbf{n}) \cdot (\gamma \times \mathbf{n}) = \alpha \mathbf{t} \cdot (\gamma \times \mathbf{n}) = \alpha \mathbf{n} \times \mathbf{t} \cdot \gamma = -\alpha \mathbf{e}_3^\top \gamma = -\alpha \\ \gamma_t \cdot (\gamma \times \mathbf{t}) = (\alpha \mathbf{t} + \beta \mathbf{n}) \cdot (\gamma \times \mathbf{t}) = \beta \mathbf{n} \cdot (\gamma \times \mathbf{t}) = \beta \mathbf{t} \times \mathbf{n} \cdot \gamma = \beta \mathbf{e}_3^\top \gamma = \beta. \end{cases} \quad (5.24)$$

So that we can write

$$\begin{cases} \alpha = -(\mathbf{\Omega}_\times \gamma) \cdot (\gamma \times \mathbf{n}) - \left(\frac{\mathbf{V}}{\rho} - \mathbf{\Omega}_\times \frac{\mathcal{T}}{\rho} + \mathcal{R} \frac{\mathbf{\Gamma}_t^w}{\rho} \right) \cdot (\gamma \times \mathbf{n}) \\ \beta = (\mathbf{\Omega}_\times \gamma) \cdot (\gamma \times \mathbf{t}) + \left(\frac{\mathbf{V}}{\rho} - \mathbf{\Omega}_\times \frac{\mathcal{T}}{\rho} + \mathcal{R} \frac{\mathbf{\Gamma}_t^w}{\rho} \right) \cdot (\gamma \times \mathbf{t}). \end{cases} \quad (5.25)$$

Since we can switch the cross and dot products in a triple scalar product, $\mathbf{\Omega} \times \gamma \cdot (\gamma \times \mathbf{n}) = \mathbf{\Omega} \cdot \gamma \times (\gamma \times \mathbf{n})$ and $\mathbf{\Omega} \times \gamma \cdot (\gamma \times \mathbf{t}) = \mathbf{\Omega} \cdot \gamma \times (\gamma \times \mathbf{t})$, giving the final result.

Corollary 2 *The spatial variation of the velocity vector field γ_t along the curve and in time can be written as*

$$\begin{aligned} \gamma_{st} &= (-\mathbf{V} + V_z \gamma) \frac{\rho_s}{\rho^2} - \frac{V_z}{\rho} \gamma_s + \mathbf{\Omega}_\times \gamma_s - (\mathbf{e}_3^\top \mathbf{\Omega}_\times \gamma_s) \gamma - (\mathbf{e}_3^\top \mathbf{\Omega}_\times \gamma) \gamma_s \\ &\quad - \frac{1}{\rho} (\mathbf{\Gamma}_{st}^w - \mathbf{e}_3^\top \mathbf{\Gamma}_{st}^w \gamma - \mathbf{e}_3^\top \mathbf{\Gamma}_t^w \gamma_s) - \frac{1}{\rho^2} (\mathbf{\Gamma}_t^w - \mathbf{e}_3^\top \mathbf{\Gamma}_t^w \gamma) \rho_s, \end{aligned} \quad (5.26)$$

and the time acceleration γ_{tt} is defined by

$$\left\{ \begin{array}{l} \mathbf{t}^\top \gamma_{tt} = \mathbf{t}^\top (\boldsymbol{\Omega}_\times^2 + [\boldsymbol{\Omega}_t]_\times) \boldsymbol{\gamma} + \frac{2}{\rho} \mathbf{t}^\top \boldsymbol{\Omega}_\times \boldsymbol{\Gamma}_t^w + \frac{1}{\rho} \mathbf{t}^\top \boldsymbol{\Gamma}_{tt}^w + \frac{1}{\rho} \mathbf{t}^\top \mathbf{V}_t \\ \quad - 2\mathbf{e}_3^\top \left(\boldsymbol{\Omega}_\times \boldsymbol{\gamma} + \frac{\mathbf{V}}{\rho} + \frac{\boldsymbol{\Gamma}_t^w}{\rho} \right) \alpha - \mathbf{e}_3^\top \left((\boldsymbol{\Omega}_\times^2 + [\boldsymbol{\Omega}_t]_\times) \boldsymbol{\gamma} + \frac{\mathbf{V}_t}{\rho} + 2\boldsymbol{\Omega}_\times \frac{\boldsymbol{\Gamma}_t^w}{\rho} + \frac{\boldsymbol{\Gamma}_{tt}^w}{\rho} \right) \mathbf{t}^\top \boldsymbol{\gamma}, \\ \mathbf{n}^\top \gamma_{tt} = \mathbf{n}^\top (\boldsymbol{\Omega}_\times^2 + [\boldsymbol{\Omega}_t]_\times) \boldsymbol{\gamma} + \frac{2}{\rho} \mathbf{n}^\top \boldsymbol{\Omega}_\times \boldsymbol{\Gamma}_t^w + \frac{1}{\rho} \mathbf{n}^\top \boldsymbol{\Gamma}_{tt}^w + \frac{1}{\rho} \mathbf{n}^\top \mathbf{V}_t \\ \quad - 2\mathbf{e}_3^\top \left(\boldsymbol{\Omega}_\times \boldsymbol{\gamma} + \frac{\mathbf{V}}{\rho} + \frac{\boldsymbol{\Gamma}_t^w}{\rho} \right) \beta - \mathbf{e}_3^\top \left((\boldsymbol{\Omega}_\times^2 + [\boldsymbol{\Omega}_t]_\times) \boldsymbol{\gamma} + \frac{\mathbf{V}_t}{\rho} + 2\boldsymbol{\Omega}_\times \frac{\boldsymbol{\Gamma}_t^w}{\rho} + \frac{\boldsymbol{\Gamma}_{tt}^w}{\rho} \right) \mathbf{n}^\top \boldsymbol{\gamma}. \end{array} \right. \quad (5.27)$$

Proof The γ_{st} expression in (5.26) is derived by differentiating γ_t with respect to s in Equation 5.3. Notice that γ_t in the moving case decomposes into the same terms as for the fixed case, Equation 5.14, plus terms dependent on $\boldsymbol{\Gamma}_t^w$ given by $\frac{1}{\rho} (\boldsymbol{\Gamma}_t^w - \mathbf{e}_3^\top \boldsymbol{\Gamma}_t^w \boldsymbol{\gamma})$. Differentiating with respect to s then gives a term equal to γ_{st} for the fixed case plus terms dependent on $\boldsymbol{\Gamma}_t^w$ and its spatial derivative, the latter being obtained by differentiating the above expression with respect to s .

The expressions of γ_{tt} in the Frenet frame were obtained by taking the dot product of (5.4) with \mathbf{t} and \mathbf{n} , noting that $\gamma_t \cdot \mathbf{t} = \alpha$ and $\gamma_t \cdot \mathbf{n} = \beta$. We then plug in expressions (5.1) and (5.2) for ρ_t and ρ_{tt} , respectively.

Special Case: Rigid Stationary Curve.

Corollary 3 (*Rigid stationary 3D curve*) Let $\boldsymbol{\Gamma}(\tilde{s})$ be a 3D curve projecting to a family of 2D curves $\boldsymbol{\gamma}(\tilde{s}, t)$ with depth $\rho(\tilde{s}, t)$, arising from camera motion with differential velocity of translation and rotation \mathbf{V} and $\boldsymbol{\Omega}$, respectively. Let \mathbf{t} denote the unit tangent to the image curve. Then

$$\gamma_{st} = \frac{-\rho_{\tilde{s}}}{\rho} \left(\frac{\mathbf{V}}{\rho} - \frac{V_z}{\rho} \boldsymbol{\gamma} \right) - \frac{V_z}{\rho} \mathbf{t} + \boldsymbol{\Omega}_\times \mathbf{t} - (\mathbf{e}_3^\top \boldsymbol{\Omega}_\times \mathbf{t}) \boldsymbol{\gamma} - (\mathbf{e}_3^\top \boldsymbol{\Omega}_\times \boldsymbol{\gamma}) \mathbf{t}. \quad (5.28)$$

Proof Follows by setting $\boldsymbol{\Gamma}_t^w = 0$ in Equation 5.26 and using the spatial parameter as the arc-length of the image curve.

Corollary 4 *The tangential and normal velocities of a rigid curve induced by a moving camera are derived from $\{\boldsymbol{\gamma}, \mathbf{t}, \mathbf{n}, \frac{\mathcal{T}}{\rho}, \boldsymbol{\Omega}, \frac{\mathbf{V}}{\rho}\}$ for any t as*

$$\left\{ \begin{array}{l} \alpha = -\boldsymbol{\Omega} \cdot \boldsymbol{\gamma} \times (\boldsymbol{\gamma} \times \mathbf{n}) - \left(\frac{\mathbf{V}}{\rho} - \boldsymbol{\Omega}_\times \frac{\mathcal{T}}{\rho} \right) \cdot \boldsymbol{\gamma} \times \mathbf{n} \\ \beta = \boldsymbol{\Omega} \cdot \boldsymbol{\gamma} \times (\boldsymbol{\gamma} \times \mathbf{t}) + \left(\frac{\mathbf{V}}{\rho} - \boldsymbol{\Omega}_\times \frac{\mathcal{T}}{\rho} \right) \cdot \boldsymbol{\gamma} \times \mathbf{t} \end{array} \right. \quad \text{for any } t, \quad (5.29)$$

$$\left\{ \begin{array}{l} \alpha = -\boldsymbol{\Omega} \cdot \boldsymbol{\gamma} \times (\boldsymbol{\gamma} \times \mathbf{n}) - \boldsymbol{\gamma} \times \mathbf{n} \cdot \frac{\mathbf{V}}{\rho} \\ \beta = \boldsymbol{\Omega} \cdot \boldsymbol{\gamma} \times (\boldsymbol{\gamma} \times \mathbf{t}) + \boldsymbol{\gamma} \times \mathbf{t} \cdot \frac{\mathbf{V}}{\rho} \end{array} \right. \quad \text{for } t = 0. \quad (5.30)$$

or

$$\left\{ \begin{array}{l} \alpha = -\boldsymbol{\Omega} \cdot \boldsymbol{\gamma} \times (\boldsymbol{\gamma} \times \mathbf{n}) - \boldsymbol{\gamma} \times \mathbf{n} \cdot \frac{\mathbf{V}}{\rho} \\ \beta = \boldsymbol{\Omega} \cdot \boldsymbol{\gamma} \times (\boldsymbol{\gamma} \times \mathbf{t}) + \boldsymbol{\gamma} \times \mathbf{t} \cdot \frac{\mathbf{V}}{\rho} \end{array} \right. \quad \text{for } t = 0. \quad (5.31)$$

$$\left\{ \begin{array}{l} \alpha = -\boldsymbol{\Omega} \cdot \boldsymbol{\gamma} \times (\boldsymbol{\gamma} \times \mathbf{n}) - \boldsymbol{\gamma} \times \mathbf{n} \cdot \frac{\mathbf{V}}{\rho} \\ \beta = \boldsymbol{\Omega} \cdot \boldsymbol{\gamma} \times (\boldsymbol{\gamma} \times \mathbf{t}) + \boldsymbol{\gamma} \times \mathbf{t} \cdot \frac{\mathbf{V}}{\rho} \end{array} \right. \quad \text{for } t = 0. \quad (5.32)$$

Proof Follows directly from Theorem 10 and $\boldsymbol{\Gamma}_t^w = 0$.

Corollary 5 *The infinitesimal Essential constraint in the Frenet frame of the image of a rigid curve is given by*

$$(\boldsymbol{\gamma} \times \mathbf{t}) \cdot \mathbf{V} [\boldsymbol{\alpha} + \boldsymbol{\Omega} \cdot \boldsymbol{\gamma} \times (\boldsymbol{\gamma} \times \mathbf{n})] + (\boldsymbol{\gamma} \times \mathbf{n}) \cdot \mathbf{V} [\boldsymbol{\beta} - \boldsymbol{\Omega} \cdot \boldsymbol{\gamma} \times (\boldsymbol{\gamma} \times \mathbf{t})] = 0. \quad (5.33)$$

Proof Eliminate ρ from (5.32) and (5.31).

Corollary 6 *(From (Papadopoulo and Faugeras 1996; Papadopoulo 1996)) The tangential velocity $\boldsymbol{\alpha}$ can be fully determined from the normal velocity $\boldsymbol{\beta}$ and $\boldsymbol{\gamma}$, \mathbf{t} , \mathbf{n} , $\boldsymbol{\Omega}$, and $\frac{\mathbf{V}}{\rho}$ without the explicit knowledge of ρ , as*

$$\boldsymbol{\alpha} = -[\boldsymbol{\beta} - \boldsymbol{\Omega} \cdot \boldsymbol{\gamma} \times (\boldsymbol{\gamma} \times \mathbf{t})] \frac{\mathbf{V} \cdot (\boldsymbol{\gamma} \times \mathbf{n})}{\mathbf{V} \cdot (\boldsymbol{\gamma} \times \mathbf{t})} - \boldsymbol{\Omega} \cdot \boldsymbol{\gamma} \times (\boldsymbol{\gamma} \times \mathbf{n}). \quad (5.34)$$

Proof Follows by solving (5.33) for $\boldsymbol{\alpha}$.

Special Case: Occluding Contours. A remarkable observation is derived below that the first-order deformation of an apparent contour under epipolar parametrization does not depend on the 3D surface geometry, since the curvature-dependent terms cancel out for an occluding contour, cf. (Cipolla and Giblin 1999).

Theorem 11 *(Occluding contours) Let $\boldsymbol{\Gamma}(s, t)$ be the contour generator for apparent contours $\boldsymbol{\gamma}(s, t)$. Then the image velocity $\boldsymbol{\gamma}_t$ at $t = 0$ can be determined from $\boldsymbol{\gamma}$ by ρ and the infinitesimal motion parameters using Equation 5.14, i.e., the same one used for a stationary contour.*

Proof Recall from Equation 2.23 that the velocity of an occluding contour under epipolar parametrization satisfies $\boldsymbol{\Gamma}_t^w = \lambda(\boldsymbol{\Gamma}^w - \mathbf{c})$ for some λ , so that at $t = 0$,

$$\boldsymbol{\Gamma}_t^w = \lambda \rho \boldsymbol{\gamma} \implies \mathbf{e}_3^\top \boldsymbol{\Gamma}_t^w = \lambda \rho, \quad (5.35)$$

so that $\boldsymbol{\Gamma}_t^w = (\mathbf{e}_3^\top \boldsymbol{\Gamma}_t^w) \boldsymbol{\gamma}$ and the terms $\boldsymbol{\Gamma}_t^w - (\mathbf{e}_3^\top \boldsymbol{\Gamma}_t^w) \boldsymbol{\gamma} = 0$ so that all appearances of $\boldsymbol{\Gamma}_t^w$ cancel-out altogether in Equation 5.3, giving exactly the same formula as for fixed contours, Equation 5.14, when $\boldsymbol{\Gamma}_t^w = 0$.

We now show exactly how the velocity of the 3D occluding contour, $\boldsymbol{\Gamma}_t^w$, depends on the curvature of the occluding surface (Cipolla 1991; Cipolla and Blake 1992).

Theorem 12 *The velocity of a 3D occluding contour under epipolar parametrization and relative to a fixed world coordinate system (camera at $t = 0$) is given by*

$$\left\{ \begin{array}{l} \boldsymbol{\Gamma}_t^w = -\frac{\mathbf{c}_t^\top \mathbf{N}^w}{K^t} \cdot \frac{\boldsymbol{\Gamma}^w - \mathbf{c}}{\|\boldsymbol{\Gamma}^w - \mathbf{c}\|^2}, \\ \boldsymbol{\Gamma}_t^w = -\frac{\mathbf{c}_t^\top \mathbf{N}}{K^t} \cdot \frac{\boldsymbol{\gamma}}{\rho \|\boldsymbol{\gamma}\|^2}, \end{array} \right. \quad \begin{array}{l} \text{for arbitrary } t, \\ \text{for } t = 0, \end{array} \quad (5.36)$$

$$\left\{ \begin{array}{l} \boldsymbol{\Gamma}_t^w = -\frac{\mathbf{c}_t^\top \mathbf{N}^w}{K^t} \cdot \frac{\boldsymbol{\Gamma}^w - \mathbf{c}}{\|\boldsymbol{\Gamma}^w - \mathbf{c}\|^2}, \\ \boldsymbol{\Gamma}_t^w = -\frac{\mathbf{c}_t^\top \mathbf{N}}{K^t} \cdot \frac{\boldsymbol{\gamma}}{\rho \|\boldsymbol{\gamma}\|^2}, \end{array} \right. \quad \begin{array}{l} \text{for arbitrary } t, \\ \text{for } t = 0, \end{array} \quad (5.37)$$

or, in terms of \mathcal{T} and \mathcal{R} , and image measurements,

$$\boldsymbol{\Gamma}_t^w = \frac{1}{K^t} \left(\frac{\mathbf{V}^\top}{\rho} \frac{\boldsymbol{\gamma} \times \mathbf{t}}{\|\boldsymbol{\gamma} \times \mathbf{t}\|} \right) \frac{\boldsymbol{\gamma}}{\|\boldsymbol{\gamma}\|^2}, \quad \text{for } t = 0, \quad (5.38)$$

where K^t is the normal curvature of the occluding surface along the visual direction.

Proof The desired *formulae* can be consistently derived by adapting variant (Astrom et al 1999) of the original result by Cipolla and Blake (Cipolla 1991; Cipolla and Blake 1992) to the proposed notation. This must be performed carefully to establish correctness in a solid way. We thus provide an alternative, clearer proof without using unit view spheres.

The normal curvature of the occluding surface along the visual direction is given by classical differential geometry (Cipolla and Giblin 1999) as

$$K^t = -\frac{\mathbf{\Gamma}_t^{w\top} \mathbf{N}_t^w}{\mathbf{\Gamma}_t^{w\top} \mathbf{\Gamma}_t^w}, \quad (5.39)$$

using epipolar parametrization. Substituting the epipolar parametrization condition of the second form of (2.23),

$$K^t = -\frac{(\mathbf{\Gamma}^w - \mathbf{c})^\top \mathbf{N}_t^w}{\lambda \|\mathbf{\Gamma}^w - \mathbf{c}\|^2}. \quad (5.40)$$

Isolating λ and plugging back into the epipolar parametrization condition,

$$\mathbf{\Gamma}_t^w = -\frac{(\mathbf{\Gamma}^w - \mathbf{c})^\top \mathbf{N}_t^w}{K^t} \frac{\mathbf{\Gamma}^w - \mathbf{c}}{\|\mathbf{\Gamma}^w - \mathbf{c}\|^2}. \quad (5.41)$$

We now show that $(\mathbf{\Gamma}^w - \mathbf{c})^\top \mathbf{N}_t^w = -\mathbf{c}_t^\top \mathbf{N}^w$, thereby arriving at the desired expression for $\mathbf{\Gamma}_t^w$. In fact, differentiating the occluding contour condition in the second form of Equation 2.22 gives

$$(\mathbf{\Gamma}_t^w - \mathbf{c}_t)^\top \mathbf{N}^w + (\mathbf{\Gamma}^w - \mathbf{c})^\top \mathbf{N}_t^w = 0, \quad (5.42)$$

$$-\mathbf{c}_t^\top \mathbf{N}^w + (\mathbf{\Gamma}^w - \mathbf{c})^\top \mathbf{N}_t^w = 0 \quad (5.43)$$

which, together with (5.41) produces the desired result

$$\mathbf{\Gamma}_t^w = -\frac{\mathbf{c}_t^\top \mathbf{N}^w}{K^t} \frac{\mathbf{\Gamma}^w - \mathbf{c}}{\|\mathbf{\Gamma}^w - \mathbf{c}\|^2}, \quad \text{for arbitrary } t. \quad (5.44)$$

At $t = 0$, we have $\mathbf{N}^w = \mathbf{N}$ and $\mathbf{\Gamma}^w - \mathbf{c} = \mathbf{\Gamma} = \rho\boldsymbol{\gamma}$ (but note that $\mathbf{\Gamma}_t(0) \neq \mathbf{\Gamma}_t^w(0)$), hence

$$\mathbf{\Gamma}_t^w = -\frac{\mathbf{c}_t^\top \mathbf{N}}{K^t} \frac{\boldsymbol{\gamma}}{\rho \|\boldsymbol{\gamma}\|^2}, \quad \text{for } t = 0. \quad (5.45)$$

Using $\mathbf{V} = -\mathbf{c}_t$ from Equation 2.12 and $\mathbf{N} = \frac{\boldsymbol{\gamma} \times \mathbf{t}}{\|\boldsymbol{\gamma} \times \mathbf{t}\|}$ gives the alternative form of this equation.

We now present a theorem relating observed quantities to camera motion, which is key for calibrating 3D motion models from families of projected deforming contours observed in video sequences with unknown camera motion, among other applications. A form of this theorem appears in (Papadopoulo and Faugeras 1996; Papadopoulo 1996), Equation L1, but this is limited to rigid motion. The following theorem generalizes the results to include occluding contours. The fact that Equation 5.46 in the theorem is also valid for occluding contours is a new result, to the best of our knowledge. The term $\mathbf{\Gamma}_t^w$ is zero for fixed contours, and is dependent on surface curvature in the case of occluding contours. The equation is not valid for arbitrary non-rigid contours because, in order to derive the normal flow equation, we used $\mathbf{\Gamma}_t^w \cdot (\boldsymbol{\gamma} \times \mathbf{t}) = 0$, which is only true for occluding and fixed contours.

Theorem 13 (A generalized form of the L1 equation of (Papadopoulo and Faugeras 1996; Papadopoulo 1996)) Given a 3D **occluding contour or fixed curve**, and the family of projected curves $\gamma(t)$ observed in a monocular sequence of images from a moving camera, and given $\mathbf{t}, \kappa, \mathbf{n}, \beta, \beta_t$ measurements at one point, then the first and second order camera motion, $\boldsymbol{\Omega}, \mathbf{V}, \boldsymbol{\Omega}_t, \mathbf{V}_t$ satisfy the polynomial equation

$$\begin{aligned} & V_z [\beta - \boldsymbol{\Omega} \cdot \boldsymbol{\gamma} \times (\boldsymbol{\gamma} \times \mathbf{t})]^2 + \mathbf{V} \cdot \boldsymbol{\gamma} \times \mathbf{t} (\beta_t - \boldsymbol{\Omega}_t \cdot \boldsymbol{\gamma} \times (\boldsymbol{\gamma} \times \mathbf{t}) - \boldsymbol{\Omega} \cdot [\boldsymbol{\gamma} \times (\boldsymbol{\gamma} \times \mathbf{t})]_t) \\ & - [\mathbf{V}_t \cdot \boldsymbol{\gamma} \times \mathbf{t} + \mathbf{V} \cdot (\boldsymbol{\gamma} \times \mathbf{t})_t] [\beta - \boldsymbol{\Omega} \cdot \boldsymbol{\gamma} \times (\boldsymbol{\gamma} \times \mathbf{t})] + \mathbf{V} \cdot \boldsymbol{\gamma} \times \mathbf{t} (\mathbf{e}_3 \cdot \boldsymbol{\Omega}_\times \boldsymbol{\gamma}) [\beta - \boldsymbol{\Omega} \cdot \boldsymbol{\gamma} \times (\boldsymbol{\gamma} \times \mathbf{t})] \\ & + \mathbf{e}_3 \cdot \boldsymbol{\Gamma}_t^w [\beta - \boldsymbol{\Omega} \cdot \boldsymbol{\gamma} \times (\boldsymbol{\gamma} \times \mathbf{t})]^2 + (\boldsymbol{\Omega}_\times \mathbf{V})(\boldsymbol{\gamma} \times \mathbf{t}) [\beta - \boldsymbol{\Omega} \cdot \boldsymbol{\gamma} \times (\boldsymbol{\gamma} \times \mathbf{t})] = 0. \end{aligned} \quad (5.46)$$

Proof The normal velocity β of an image contour follows Equation (5.30), which holds for both stationary curves, Corollary 4, and for occluding contours, Theorem 11. Differentiating it with respect to time,

$$\begin{aligned} \rho_t \beta + \beta_t \rho = & \rho_t \boldsymbol{\Omega} \cdot \boldsymbol{\gamma} \times (\boldsymbol{\gamma} \times \mathbf{t}) + \rho \boldsymbol{\Omega}_t \cdot \boldsymbol{\gamma} \times (\boldsymbol{\gamma} \times \mathbf{t}) + \rho \boldsymbol{\Omega} [\boldsymbol{\gamma} \times (\boldsymbol{\gamma} \times \mathbf{t})]_t \\ & + (\boldsymbol{\gamma} \times \mathbf{t})_t (\mathbf{V} - \boldsymbol{\Omega}_\times \boldsymbol{\mathcal{T}}) + (\boldsymbol{\gamma} \times \mathbf{t}) (\mathbf{V}_t - \boldsymbol{\Omega}_t \times \boldsymbol{\mathcal{T}} - \boldsymbol{\Omega}_\times \mathbf{V}) \end{aligned} \quad (5.47)$$

Rearranging the terms,

$$\begin{aligned} & \rho_t [\beta - \boldsymbol{\Omega} \cdot \boldsymbol{\gamma} \times (\boldsymbol{\gamma} \times \mathbf{t})] + \rho [\beta_t - \boldsymbol{\Omega}_t \cdot \boldsymbol{\gamma} \times (\boldsymbol{\gamma} \times \mathbf{t}) - \boldsymbol{\Omega} \cdot [\boldsymbol{\gamma} \times (\boldsymbol{\gamma} \times \mathbf{t})]_t] \\ & = (\boldsymbol{\gamma} \times \mathbf{t})_t (\mathbf{V} - \boldsymbol{\Omega}_\times \boldsymbol{\mathcal{T}}) + (\boldsymbol{\gamma} \times \mathbf{t}) (\mathbf{V}_t - \boldsymbol{\Omega}_t \times \boldsymbol{\mathcal{T}} - \boldsymbol{\Omega}_\times \mathbf{V}). \end{aligned} \quad (5.48)$$

Setting $t = 0$,

$$\begin{aligned} & \rho_t [\beta - \boldsymbol{\Omega} \cdot \boldsymbol{\gamma} \times (\boldsymbol{\gamma} \times \mathbf{t})] + \rho [\beta_t - \boldsymbol{\Omega}_t \cdot \boldsymbol{\gamma} \times (\boldsymbol{\gamma} \times \mathbf{t}) - \boldsymbol{\Omega} \cdot [\boldsymbol{\gamma} \times (\boldsymbol{\gamma} \times \mathbf{t})]_t] \\ & = (\boldsymbol{\gamma} \times \mathbf{t})_t \mathbf{V} + (\boldsymbol{\gamma} \times \mathbf{t}) (\mathbf{V}_t - \boldsymbol{\Omega}_\times \mathbf{V}) \end{aligned} \quad (5.49)$$

Now, from Equation 5.1, we can plug-in an expression for ρ_t at $t = 0$,

$$\begin{aligned} & (\rho \mathbf{e}_3^\top \boldsymbol{\Omega}_\times \boldsymbol{\gamma} + V_z + \mathbf{e}_3^\top \boldsymbol{\Gamma}_t^w) [\beta - \boldsymbol{\Omega} \cdot \boldsymbol{\gamma} \times (\boldsymbol{\gamma} \times \mathbf{t})] + \rho (\beta_t - \boldsymbol{\Omega}_t \cdot \boldsymbol{\gamma} \times (\boldsymbol{\gamma} \times \mathbf{t}) - \boldsymbol{\Omega} \cdot [\boldsymbol{\gamma} \times (\boldsymbol{\gamma} \times \mathbf{t})]_t) \\ & = (\boldsymbol{\gamma} \times \mathbf{t})_t \mathbf{V} + (\boldsymbol{\gamma} \times \mathbf{t}) (\mathbf{V}_t - \boldsymbol{\Omega}_\times \mathbf{V}), \end{aligned} \quad (5.50)$$

which is analogous to Equation 7.28 of (Papadopoulo 1996, p.167), but this time with occluding contours also being included. Now, eliminating depth ρ using Equation 5.32, *e.g.*, by multiplying the above by $[\beta - \boldsymbol{\Omega} \cdot \boldsymbol{\gamma} \times (\boldsymbol{\gamma} \times \mathbf{t})]$, we obtain

$$\begin{aligned} & [V_z (\beta - \boldsymbol{\Omega} \cdot \boldsymbol{\gamma} \times (\boldsymbol{\gamma} \times \mathbf{t})) + (\mathbf{V} \cdot \boldsymbol{\gamma} \times \mathbf{t}) \mathbf{e}_3 \cdot \boldsymbol{\Omega}_\times \boldsymbol{\gamma} + \\ & \mathbf{e}_3 \cdot \boldsymbol{\Gamma}_t^w (\beta - \boldsymbol{\Omega} \cdot \boldsymbol{\gamma} \times (\boldsymbol{\gamma} \times \mathbf{t}))] [\beta - \boldsymbol{\Omega} \cdot \boldsymbol{\gamma} \times (\boldsymbol{\gamma} \times \mathbf{t})] \\ & + \mathbf{V} \cdot \boldsymbol{\gamma} \times \mathbf{t} [\beta_t - \boldsymbol{\Omega}_t \cdot \boldsymbol{\gamma} \times (\boldsymbol{\gamma} \times \mathbf{t}) - \boldsymbol{\Omega} \cdot [\boldsymbol{\gamma} \times (\boldsymbol{\gamma} \times \mathbf{t})]_t] = \\ & [\mathbf{V}_t \cdot \boldsymbol{\gamma} \times \mathbf{t} + \mathbf{V} (\boldsymbol{\gamma} \times \mathbf{t})_t - (\boldsymbol{\Omega}_\times \mathbf{V})(\boldsymbol{\gamma} \times \mathbf{t})] [\beta - \boldsymbol{\Omega} \cdot \boldsymbol{\gamma} \times (\boldsymbol{\gamma} \times \mathbf{t})]. \end{aligned} \quad (5.51)$$

Rearranging the terms, we obtain the desired equation.

Remark 2 Note that previously reported results for the rigid case (Papadopoulo 1996, eq. 7.12) have an apparently missing term corresponding to the last term in our Equation 5.46,

$$(\boldsymbol{\Omega}_\times \mathbf{V})(\boldsymbol{\gamma} \times \mathbf{t}) [\beta - \boldsymbol{\Omega} \cdot \boldsymbol{\gamma} \times (\boldsymbol{\gamma} \times \mathbf{t})].$$

This is due to the fact that they used slightly different variables for the translational component of the infinitesimal motion equations, but the results are mathematically the same for the rigid case.

Theorem 14 *The first spatial derivative of image apparent motion of both a fixed curve and an occluding contour under epipolar correspondence is given by*

$$\gamma_{st} = \left(-\frac{\mathbf{V}}{\rho} + \frac{V_z}{\rho} \gamma \right) \frac{\rho_s}{\rho} - \frac{V_z}{\rho} \gamma_s + \boldsymbol{\Omega}_\times \gamma_s - (\mathbf{e}_3^\top \boldsymbol{\Omega}_\times \gamma_s) \gamma - (\mathbf{e}_3^\top \boldsymbol{\Omega}_\times \gamma) \gamma_s. \quad (5.52)$$

Note that the derivative of depth ρ_s can be expressed in terms of 3D curve geometry as $\rho_s = \mathbf{e}_3^\top \boldsymbol{\Gamma}_s$.

Proof Equation 5.52 follows by differentiating the fixed flow (5.14) with respect to s , observing that only ρ and γ depend on s . The formula for ρ_s is obtained from the observation that the dot product of $\boldsymbol{\Gamma} = \rho \gamma$ with \mathbf{e}_3 gives $\mathbf{e}_3^\top \boldsymbol{\Gamma} = \rho$. Differentiating this with respect to s gives $\rho_s = \mathbf{e}_3^\top \boldsymbol{\Gamma}_s$.

Theorem 9 gives an expression for the image acceleration of a moving 3D point, which includes points lying on any type of contour (even non-rigid), in terms of the evolution of the 3D curve. Since the latter is expressed in terms of a fixed world coordinate system, the motion of the object and the motion of the cameras are written down separately, even though they exert joint effects on image velocity.

Theorem 15 *The image acceleration of an occluding contour under epipolar parametrization is given by*

$$\begin{aligned} \gamma_{tt} = & (\boldsymbol{\Omega}_\times^2 + [\boldsymbol{\Omega}_t]_\times) \gamma - [\mathbf{e}_3^\top (\boldsymbol{\Omega}_\times^2 + [\boldsymbol{\Omega}_t]_\times) \gamma] \gamma + 2 \boldsymbol{\Omega}_\times \frac{\boldsymbol{\Gamma}_t^w}{\rho} + \frac{\mathbf{V}_t}{\rho} - \frac{2\rho_t}{\rho} \gamma_t + \frac{\mathbf{e}_3^\top \boldsymbol{\Gamma}_t^w}{\rho} \gamma_t \\ & - \frac{\mathbf{e}_3^\top \boldsymbol{\Gamma}_t^w}{\rho} \boldsymbol{\Omega}_\times \gamma - \frac{\mathbf{e}_3^\top \mathbf{V}_t}{\rho} \gamma - \frac{2\mathbf{e}_3^\top \boldsymbol{\Omega}_\times \boldsymbol{\Gamma}_t^w}{\rho} \gamma + \frac{(\mathbf{e}_3^\top \boldsymbol{\Gamma}_t^w)(\mathbf{e}_3^\top \boldsymbol{\Omega}_\times \gamma)}{\rho} \gamma \quad \text{at } t = 0, \end{aligned} \quad (5.53)$$

where γ_t and ρ_t are given by Equations 5.14 and 5.13, and $\boldsymbol{\Gamma}_t^w$ is dependent on curvature, Equation 5.38.

Proof Substituting Equation 5.2 into Equation 5.12, we get

$$\gamma_{tt} = (\boldsymbol{\Omega}_\times^2 + [\boldsymbol{\Omega}_t]_\times) \gamma + \frac{2\boldsymbol{\Omega}_\times \boldsymbol{\Gamma}_t^w}{\rho} + \frac{\boldsymbol{\Gamma}_{tt}^w}{\rho} + \frac{\mathbf{V}_t}{\rho} - \frac{2\rho_t \gamma_t}{\rho} - [\mathbf{e}_3^\top (\boldsymbol{\Omega}_\times^2 + [\boldsymbol{\Omega}_t]_\times) \gamma] \gamma - \frac{\mathbf{e}_3^\top \mathbf{V}_t}{\rho} \gamma - \frac{2\mathbf{e}_3^\top \boldsymbol{\Omega}_\times \boldsymbol{\Gamma}_t^w}{\rho} \gamma - \frac{\mathbf{e}_3^\top \boldsymbol{\Gamma}_{tt}^w}{\rho} \gamma. \quad (5.54)$$

Now, let \mathbf{v} be the viewing direction in world coordinates, so that

$$\gamma = \mathcal{R} \mathbf{v}, \quad (5.55)$$

and let \mathbf{f} be the normal to the image plane in world coordinates, so that

$$\mathbf{e}_3 = \mathcal{R} \mathbf{f}. \quad (5.56)$$

Thus,

$$\mathbf{e}_3^\top \gamma = \mathbf{f}^\top \mathcal{R}^\top \mathcal{R} \mathbf{v} = \mathbf{f}^\top \mathbf{v} = 1. \quad (5.57)$$

Note also that at $t = 0$ we have $\mathbf{f} = \mathbf{e}_3$ and $\gamma = \mathbf{v}$. Now, the condition for epipolar parametrization of an occluding contour, Equation 2.23, can be expressed as

$$\boldsymbol{\Gamma}_t^w = \lambda \mathbf{v}, \quad (5.58)$$

for some scalar factor λ . Taking the dot product with \mathbf{f} we have

$$\begin{cases} \lambda = \mathbf{f}^\top \mathbf{\Gamma}_t^w, \\ \mathbf{\Gamma}_t^w = \mathbf{f}^\top \mathbf{\Gamma}_t^w \mathbf{v}. \end{cases} \quad (5.59)$$

$$\mathbf{\Gamma}_t^w = \mathbf{f}^\top \mathbf{\Gamma}_t^w \mathbf{v}. \quad (5.60)$$

Differentiating (5.58) with respect to time and using (5.59) gives

$$\mathbf{\Gamma}_{tt}^w = \lambda_t \mathbf{v} + \lambda \mathbf{v}_t = \lambda_t \mathbf{v} + \mathbf{f}^\top \mathbf{\Gamma}_t^w \mathbf{v}_t. \quad (5.61)$$

Taking the dot product with \mathbf{f} ,

$$\mathbf{f}^\top \lambda_t \mathbf{v} + \mathbf{f}^\top (\mathbf{f}^\top \mathbf{\Gamma}_t^w) \mathbf{v}_t = \mathbf{f}^\top \mathbf{\Gamma}_{tt}^w \quad (5.62)$$

$$\lambda_t = \mathbf{f}^\top \mathbf{\Gamma}_{tt}^w - (\mathbf{f}^\top \mathbf{\Gamma}_t^w) \mathbf{f}^\top \mathbf{v}_t. \quad (5.63)$$

Thus,

$$\mathbf{\Gamma}_{tt}^w = (\mathbf{f}^\top \mathbf{\Gamma}_{tt}^w) \mathbf{v} - (\mathbf{f}^\top \mathbf{\Gamma}_t^w) (\mathbf{f}^\top \mathbf{v}_t) \mathbf{v} + (\mathbf{f}^\top \mathbf{\Gamma}_t^w) \mathbf{v}_t, \quad (5.64)$$

$$\mathbf{\Gamma}_{tt}^w = \mathbf{e}_3^\top \mathbf{\Gamma}_{tt}^w \boldsymbol{\gamma} - (\mathbf{e}_3^\top \mathbf{\Gamma}_t^w) (\mathbf{e}_3^\top \mathbf{v}_t) \boldsymbol{\gamma} + \mathbf{e}_3^\top \mathbf{\Gamma}_t^w \mathbf{v}_t \quad \text{at } t = 0. \quad (5.65)$$

In order to get $\mathbf{v}_t(0)$ in terms of $\boldsymbol{\gamma}$ we write

$$\boldsymbol{\gamma}_t = \mathcal{R}_t \mathbf{v} + \mathcal{R} \mathbf{v}_t. \quad (5.66)$$

Thus

$$\mathbf{v}_t = \boldsymbol{\gamma}_t - \boldsymbol{\Omega}_\times \boldsymbol{\gamma} \quad \text{at } t = 0. \quad (5.67)$$

Substituting back into (5.65),

$$\mathbf{\Gamma}_{tt}^w = \mathbf{e}_3^\top \mathbf{\Gamma}_{tt}^w \boldsymbol{\gamma} + \mathbf{e}_3^\top \mathbf{\Gamma}_t^w \boldsymbol{\gamma}_t - \mathbf{e}_3^\top \mathbf{\Gamma}_t^w \boldsymbol{\Omega}_\times \boldsymbol{\gamma} + (\mathbf{e}_3^\top \mathbf{\Gamma}_t^w) (\mathbf{e}_3^\top \boldsymbol{\Omega}_\times \boldsymbol{\gamma}) \boldsymbol{\gamma} \quad \text{at } t = 0. \quad (5.68)$$

Plugging this equation onto (5.54), the $\mathbf{e}_3^\top \mathbf{\Gamma}_{tt}^w \boldsymbol{\gamma} / \rho$ terms cancel out, giving the final equation.

6 Mathematical Experiment

To illustrate and test the proposed theoretical framework, we have devised an experiment around a synthetic dataset constructed for this research. This dataset has already been used for validating a pose estimation system (Fabbri et al 2012). The dataset is composed of the following components:

1. A variety of synthetically generated 3D curves (helices, parabolas, ellipses, straight lines, and saddle curves) with well-known parametric equations, as shown in Figure 5.
2. Ground-truth camera models for a video sequence around the curves.
3. Differential geometry of the space curves analytically computed up to third-order (torsion and curvature derivative), using Maple when necessary. The dataset together with C++ code implementing these expressions from Maple are listed in the supplementary material Online Resource 1.
4. The 3D curves are densely sampled, each 3D sample having attributed differential geometry from the analytic computation (up to torsion and curvature).
5. A video sequence containing a family of 2D curve samples with attributed differential geometry is rendered by projecting the 3D samples onto a 500×400 view using the ground truth cameras. These subpixel edgels with attributed differential geometry simulate ideal aspects of what in practice could be the output of high-quality subpixel edge detection and grouping (Tamrakar and Kimia 2007; Tamrakar 2008; Guo et al 2014).

6. Correspondence between all samples obtained by keeping track of the underlying 3D points.
7. Specific analytic expressions for 2D differential geometry were derived using Maple since these are often too long due to perspective projection. These expressions are also provided in the C++ code that synthesizes the dataset.
8. C++ code implementing the formulas in this paper is also provided with the dataset, and can be readily used in other projects.

For the present theoretical paper, the experiments consist of checking the proposed expressions against the analytic expressions that are obtained by differentiating each specific parametric equation. After projecting differential geometry using our formulas applied to the 3D samples attributed with differential geometry, we obtain corresponding 2D projected differential geometry at each sample. We compare this to the differential geometry on the curve projections analytically computed from the parametric equations, observing a match. We then reconstruct these correspondences up to third-order differential geometry using the proposed expressions, and observe that they indeed match to the original analytic expressions from Maple. We have also performed a similar experiment for the expressions involving occluding contours, using a 3D ellipsoid and sphere.

We have observed a complete agreement between our code and the specific analytic expressions, confirming that the formulas as presented in this manuscript are correct. The source code of this illustrative experiment also serves as an example of how to use the proposed framework in programming practice, how to check for degenerate conditions stated in the theorems, among others.

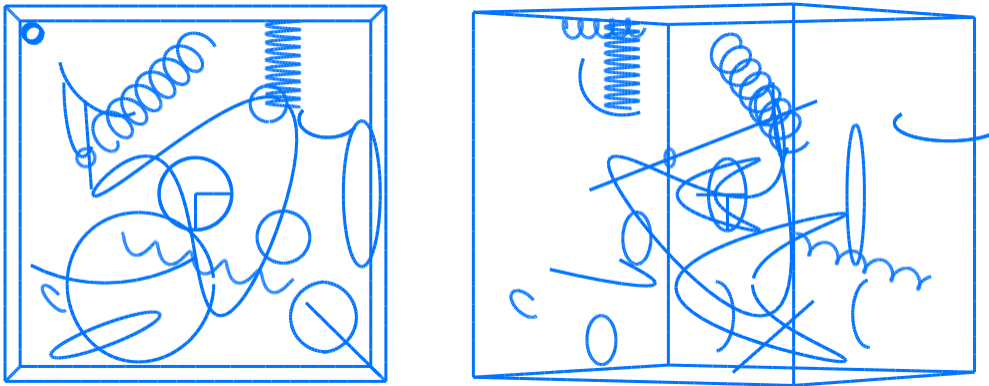


Fig. 5: Two views of the synthetic multiview curve differential geometry dataset (Fabbri et al 2012).

7 Conclusion

We presented a unified differential-geometric theory of projection and reconstruction of general curves from multiple views. By gathering previously scattered results using a coherent notation and proof methodology that scale to expressing more sophisticated ideas, we were able to prove novel results and to provide a comprehensive study on how the differential geometry of curves behaves under perspective projection, including the effects of intrinsic parameters. For instance, we derived how the tangent, curvature, and curvature derivative of a space curve projects onto an image, and

how the motion of the camera and of the curve relates to the projections. This leads to the *novel* result that torsion – which characterizes the tri-dimensionality of space curves – projects to curvature derivative in an image, and the *novel* result of how the parametrization of corresponding image curves are linked across different views, up to third order to reflect the underlying torsion. We also proved formulas for reconstructing differential geometry, given differential geometry at corresponding points measured in at least two views. In particular, this gives the *novel* result of reconstructing space curve torsion, given corresponding points, tangents, curvatures, and curvature derivatives measured in two views. We determined that there are no correspondence constraints in two views – any pair of points with attributed tangents, curvatures, and curvature derivatives are possible matches, as long as the basic point epipolar constraint is satisfied. There is, however, a constraint in three or more views: from two views one can transfer differential geometry onto other views and enforce measurements to match the reprojections using local curve shape, avoiding clutter. This has been demonstrated in a recent work in curve-based multiview stereo by the authors (Fabbri and Kimia 2010; Usumezbas et al 2016), namely for matching linked curve fragments from a subpixel edge detector across many views. Experiments clearly show that differential-geometric curve structure is essential for the matching to be immune to edge clutter and linking instability, by enforcing reprojections to match to image data in *local* shape.

This paper is part of a greater effort of augmenting multiple view geometry to model general curved structures (Fabbri 2010). Work on camera pose estimation based on curves using the formulas in this paper has been recently published (Fabbri et al 2012), and trifocal relative pose estimation using local curve geometry to bootstrap the system is currently under investigation. In a complete system, once a core set of three views are estimated and an initial set of curves are reconstructed, more views can be iteratively registered (Fabbri et al 2012). These applications of the theory presented in this paper and their ongoing extensions would enable a practical structure from motion pipeline based on curve fragments, complementing interest point technology. We have also been working on the multiview differential geometry of surfaces and their shading.

References

- Agarwal S, Snavely N, Simon I, Seitz SM, Szeliski R (2009) Building Rome in a day. In: Proceedings of the IEEE International Conference on Computer Vision, IEEE Computer Society 2, 3
- Arnold R, Binford T (1980) Geometric constraints in stereo vision. In: Proc. SPIE, San Diego, CA, vol 238–Image Processing for Missile Guidance, pp 281–292 4
- Astrom K, Heyden A (1996) Multilinear constraints in the infinitesimal-time case. In: Proceedings of the IEEE Computer Society Conference on Computer Vision and Pattern Recognition, IEEE Computer Society Press, San Francisco, California, pp 833–838 18
- Åström K, Heyden A (1998) Continuous time matching constraints for image streams. *International Journal of Computer Vision* 28(1):85–96, DOI 10.1023/A:1008006815607, URL <http://dx.doi.org/10.1023/A:1008006815607> 20
- Astrom K, Kahl F (1999) Motion estimation in image sequences using the deformation of apparent contours. *IEEE Trans Pattern Anal Mach Intell* 21(2):114–127, DOI <http://dx.doi.org/10.1109/34.748821> 4
- Astrom K, Cipolla R, Giblin P (1999) Generalised epipolar constraints. *Int J Comput Vision* 33(1):51–72, DOI <http://dx.doi.org/10.1023/A:1008113231241> 4, 24
- Ayache N, Lustman L (1987) Fast and reliable passive trinocular stereovision. In: 1st International Conference on Computer Vision 4
- Baatz G, Saurer O, Köser K, Pollefeys M (2012) Large scale visual geo-localization of images in mountainous terrain. In: Proceedings of the 12th European Conference on Computer Vision - Volume Part II, Springer-Verlag, Berlin, Heidelberg, ECCV'12, pp 517–530, DOI 10.1007/978-3-642-33709-3_37, URL http://dx.doi.org/10.1007/978-3-642-33709-3_37 3

- Baumela L, Agapito L, Bustos P, Reid I (2000) Motion estimation using the differential epipolar equation. Proceedings of the 15th International Conference on Pattern Recognition 3:848–851 18
- Berthilsson R, Åström K, Heyden A (2001) Reconstruction of general curves, using factorization and bundle adjustment. *International Journal of Computer Vision* 41(3):171–182, DOI <http://dx.doi.org/10.1023/A:10111040205864>
- Brodský T, Fermüller C (2002) Self-Calibration from Image Derivatives. *International Journal of Computer Vision* 48(2):91–114 18
- Brodský T, Fermüller C, Aloimonos Y (2000) Structure from motion: Beyond the epipolar constraint. *Int J Comput Vision* 37(3):231–258, DOI <http://dx.doi.org/10.1023/A:1008132107950> 18
- Brooks MJ, Chojnacki W, Baumela L (1997) Determining the egomotion of an uncalibrated camera from instantaneous optical flow. *J Opt Soc Am A* 14(10):2670–2677, DOI 10.1364/JOSAA.14.002670, URL <http://josaa.osa.org/abstract.cfm?URI=josaa-14-10-2670> 19
- Calakli F, Ulusoy AO, Restrepo MI, Taubin G, Mundy JL (2012) High resolution surface reconstruction from multi-view aerial imagery. In: 3DIMPVT'12, IEEE, pp 25–32 3
- Carceroni R (2001) Recovering non-rigid 3D motion, shape and reflectance from multi-view image sequences: A differential-geometric approach. PhD thesis, University of Rochester 18
- Carceroni R, Kutulakos K (1999) Toward recovering shape and motion of 3D curves from multi-view image sequences. In: Proceedings of the IEEE Computer Society Conference on Computer Vision and Pattern Recognition, IEEE Computer Society Press, Fort Collins, Colorado, USA, pp 23–25 18
- do Carmo MP (1976) *Differential Geometry of Curves and Surfaces*. Prentice-Hall, New Jersey 5
- Chen TY, Klette R (2014) Animated non-photorealistic rendering in multiple styles. In: Image and Video Technology—PSIVT 2013 Workshops, Springer, pp 12–23 4
- Cipolla R (1991) Active visual inference of surface shape. Ph.D. dissertation, University of Oxford 17, 18, 23, 24
- Cipolla R, Blake A (1992) Surface shape from the deformation of apparent contours. *International Journal of Computer Vision* 9(2):83–112 18, 23, 24
- Cipolla R, Giblin P (1999) *Visual Motion of Curves and Surfaces*. Cambridge University Press 4, 5, 10, 13, 18, 23, 24
- Cipolla R, Zisserman A (1992) Qualitative surface shape from deformation of image curves. *International Journal of Computer Vision* 8(1):53–69 13
- Cipolla R, Åström K, Giblin PJ (1995) Motion from the frontier of curved surfaces. In: Proceedings of the IEEE International Conference on Computer Vision, IEEE Computer Society Press, Boston, Massachusetts, pp 269–275 4
- Cole F, Sanik K, DeCarlo D, Finkelstein A, Funkhouser T, Rusinkiewicz S, Singh M (2009) How well do line drawings depict shape? In: ACM Transactions on Graphics (Proc. SIGGRAPH) 4
- Diskin Y, Asari V (2015) Dense point-cloud representation of a scene using monocular vision. *Journal of Electronic Imaging* 24(2):023,003, DOI 10.1117/1.JEI.24.2.023003, URL <http://dx.doi.org/10.1117/1.JEI.24.2.023003> 3
- Dornaika F, Sappa A (2006) 3D Motion from Image Derivatives Using the Least Trimmed Square Regression? *LECTURE NOTES IN COMPUTER SCIENCE* 4153:76 18
- Fabbri R (2010) Multiview differential geometry in application to computer vision. Ph.D. dissertation, Division Of Engineering, Brown University, Providence, RI, 02912 29
- Fabbri R, Kimia BB (2010) 3D curve sketch: Flexible curve-based stereo reconstruction and calibration. In: Proceedings of the IEEE Conference on Computer Vision and Pattern Recognition, IEEE Computer Society Press, San Francisco, CA, USA 3, 5, 29
- Fabbri R, Kimia BB, Giblin PJ (2012) Camera pose estimation using first-order curve differential geometry. In: Proceedings of European Conference on Computer Vision, Springer, Lecture Notes in Computer Science, pp 231–244 3, 5, 27, 28, 29
- Fathi H, Dai F, Lourakis M (2015) Automated as-built 3D reconstruction of civil infrastructure using computer vision: Achievements, opportunities, and challenges. *Advanced Engineering Informatics* (0):–, DOI <http://dx.doi.org/10.1016/j.aei.2015.01.012>, URL <http://www.sciencedirect.com/science/article/pii/S1474034615000245> 3
- Faugeras O (1990) *Computer Vision — ECCV 90: First European Conference on Computer Vision* Antibes, France, April 23–27, 1990 Proceedings, Springer Berlin Heidelberg, Berlin, Heidelberg, chap On the motion of 3D curves and its relationship to optical flow, pp 105–117. DOI 10.1007/BFb0014856, URL <http://dx.doi.org/10.1007/BFb0014856> 18
- Faugeras O, Papadopoulos T (1992) *Geometric invariance in computer vision*. MIT Press, Cambridge, MA, USA, chap Disambiguating Stereo Matches with Spatio-temporal Surfaces, pp 310–331, URL <http://dl.acm.org/citation.cfm?id=153634.153650> 4
- Faugeras O, Papadopoulos T (1993) A theory of the motion fields of curves. *International Journal of Computer Vision* 10(2):125–156 4, 16, 18

- Fischler MA, Bolles RC (1981) Random sample consensus: a paradigm for model fitting with applications to image analysis and automated cartography. *Commun ACM* 24(6):381–395, DOI <http://doi.acm.org/10.1145/358669.358692> 3
- Furukawa Y, Ponce J (2007) Accurate, dense, and robust multi-view stereopsis. In: *Proceedings of the IEEE Computer Society Conference on Computer Vision and Pattern Recognition*, IEEE Computer Society 3
- Furukawa Y, Ponce J (2010) Accurate, dense, and robust multiview stereopsis. *IEEE Transactions on Pattern Analysis and Machine Intelligence* 32:1362–1376, DOI <http://doi.ieeecomputersociety.org/10.1109/TPAMI.2009.161> 3
- Furukawa Y, Sethi A, Ponce J, Kriegman DJ (2006) Robust structure and motion from outlines of smooth curved surfaces. *IEEE Trans Pattern Anal Mach Intell* 28(2):302–315 4
- Giblin PJ, Weiss RS (1995) Epipolar curves on surfaces. *Image and Vision Computing* 13(1):33–44 10
- Goesele M, Snavely N, Curless B, Hoppe H, Seitz S (2007) Multi-view stereo for community photo collections. In: *(ICCV2007 2007)*, pp 1–8 3
- Grimson WEL (1981) *A Computer Implementation of a Theory of Human Stereo Vision*. Royal Society of London Philosophical Transactions Series B 292:217–253 4
- Guo Y, Kumar N, Narayanan M, Kimia B (2014) A multi-stage approach to curve extraction. In: *CVPR'14* 27
- Habbecke M, Kobbelt L (2007) A surface-growing approach to multi-view stereo reconstruction. *Computer Vision and Pattern Recognition*, IEEE Computer Society Conference on 0:1–8, DOI <http://doi.ieeecomputersociety.org/10.1109/CVPR.2007.383195> 3
- Harris C, Stephens M (1988) A combined edge and corner detector. In: *Alvey Vision Conference*, pp 189–192 2
- Hartley R, Zisserman A (2000) *Multiple View Geometry in Computer Vision*. Cambridge University Press 3
- Hartley RI (1995) A linear method for reconstruction from lines and points. In: *Proceedings of the IEEE International Conference on Computer Vision*, IEEE Computer Society Press, Boston, Massachusetts, pp 882–887 4
- Heeger DJ, Jepson AD (1992) Subspace methods for recovering rigid motion i: algorithm and implementation. *Int J Comput Vision* 7(2):95–117, DOI <http://dx.doi.org/10.1007/BF00128130> 20
- Heinly J, Schönberger JL, Dunn E, Frahm JM (2015) Reconstructing the world in six days. In: *Computer Vision and Pattern Recognition* 2, 3
- van den Hengel A (2000) *Robust estimation of structure from motion in the uncalibrated case*. PhD thesis, Adelaide University 18
- van den Hengel A, Chojnacki W, Brooks M (2007) Determining the Translational Speed of a Camera from Time-Varying Optical Flow. *LECTURE NOTES IN COMPUTER SCIENCE* 3417:190 18
- Hernandez C, Schmitt F, Cipolla R (2007) Silhouette coherence for camera calibration under circular motion. *IEEE Trans Pattern Anal Mach Intell* 29(2):343–349 4
- Hernández Esteban C, Schmitt F (2004) Silhouette and stereo fusion for 3D object modeling. *Computer Vision and Image Understanding* 96(3):367–392 3
- Heyden A (2006) *Differential-Algebraic Multiview Constraints*. In: *Proceedings of the 18th International Conference on Pattern Recognition (ICPR'06)-Volume 01*, IEEE Computer Society Washington, DC, USA, pp 159–162 18
- ICCV2007 (2007) *11th IEEE International Conference on Computer Vision (ICCV 2007)*, 14–20 October 2007, Rio de Janeiro, Brazil, IEEE Computer Society 31, 33
- Jain V (2009) *Motion segmentation using differential geometry of curves and edges*. Ph.D. dissertation, Division Of Engineering, Brown University, Providence, RI, 02912 5
- Jain V, Kimia BB, Mundy JL (2007a) Background modeling based on subpixel edges. In: *IEEE International Conference on Image Processing*, IEEE, San Antonio, TX, USA, vol IV, pp 321–324 5
- Jain V, Kimia BB, Mundy JL (2007b) Segregation of moving objects using elastic matching. *Computer Vision and Image Understanding* 108:230–242 5
- Kahl F, Heyden A (1998) Using conic correspondence in two images to estimate the epipolar geometry. In: *Proceedings of the IEEE International Conference on Computer Vision*, IEEE Computer Society Press, Bombay, India, p 761 4
- Kahl F, Heyden A (2001) Euclidean reconstruction and auto-calibration from continuous motion. In: *Proceedings of the IEEE International Conference on Computer Vision*, IEEE Computer Society Press, Vancouver, Canada, vol 2 18
- Kaminski JY, Shashua A (2004) Multiple view geometry of general algebraic curves. *International Journal of Computer Vision* 56(3):195–219 4
- Kanatani K (1993) 3-d interpretation of optical flow by renormalization. *International Journal of Computer Vision* 11(3):267–282, DOI 10.1007/BF01469345, URL <http://dx.doi.org/10.1007/BF01469345> 19
- Kazhdan M, Bolitho M, Hoppe H (2006) Poisson surface reconstruction. In: *SGP '06: Proceedings of the fourth Eurographics symposium on Geometry processing*, Eurographics Association, Aire-la-Ville, Switzerland, Switzerland, pp 61–70 3
- Koenderink J, van Doorn A, Wagemans J (2013) Sfs? not likely... *i-Perception* 4(5):299 4

- Kowdle A, Batra D, Chen WC, Chen T (2012) imodel: Interactive co-segmentation for object of interest 3D modeling. In: Proceedings of the 11th European Conference on Trends and Topics in Computer Vision - Volume Part II, Springer-Verlag, ECCV'10, pp 211–224, DOI 10.1007/978-3-642-35740-4_17, URL http://dx.doi.org/10.1007/978-3-642-35740-4_17 4
- Kuang Y, Åström K (2013) Pose estimation with unknown focal length using points, directions and lines. In: International Conference on Computer Vision, IEEE, pp 529–536 5
- Kuang Y, Oskarsson M, Åström K (2014) Revisiting trifocal tensor estimation using lines. In: Pattern Recognition (ICPR), 2014 22nd International Conference on, IEEE, pp 2419–2423 5
- Kunsberg B, Zucker SW (2014) Why shading matters along contours. In: Neuromathematics of Vision, Lecture Notes in Morphogenesis, Springer, pp 107–129, DOI 10.1007/978-3-642-34444-2_3, URL http://dx.doi.org/10.1007/978-3-642-34444-2_3 4
- Lebeda K, Hadfield S, Bowden R (2014) 2D or not 2D: Bridging the gap between tracking and structure from motion. In: Proc. of ACCV 3
- Li G, Zucker SW (2003) A differential geometrical model for contour-based stereo correspondence. In: Proc. IEEE Workshop on Variational, Geometric, and Level Set Methods in Computer Vision, Nice, France 4, 13, 17
- Li G, Zucker SW (2006) Contextual inference in contour-based stereo correspondence. International Journal of Computer Vision 69(1):59–75 17
- Lin WY, Tan GC, Cheong LF (2009) When discrete meets differential. International Journal of Computer Vision 86(1):87–110, DOI 10.1007/s11263-009-0260-y, URL <http://dx.doi.org/10.1007/s11263-009-0260-y> 20
- Litvinov V, Yu S, Lhuillier M (2012) 2-manifold reconstruction from sparse visual features. In: 3D Imaging (IC3D), 2012 International Conference on, IEEE, pp 1–8 3
- Longuet-Higgins HC (1981) A computer algorithm for reconstructing a scene from two projections. Nature 293:133–135 19
- Longuet-Higgins HC, Prazdny K (1980) The interpretation of a moving retinal image. Proc R Society London 208(1173):385–397 18, 19
- Lowe DG (2004) Distinctive image features from scale-invariant keypoints. Int Journal of Computer Vision 60(2):91–110 2
- Ma Y, Soatto S, Kosecka J, Sastry SS (2004) An invitation to 3D vision. Springer 18, 20
- Mattingly WA, Chariker JH, Paris R, Jen Chang D, Pani JR (2015) 3D modeling of branching structures for anatomical instruction. Journal of Visual Languages & Computing 29(0):54–62, DOI <http://dx.doi.org/10.1016/j.jvlc.2015.02.006>, URL <http://www.sciencedirect.com/science/article/pii/S1045926X15000191> 4
- Maybank S (1992) Theory of Reconstruction from Image Motion. Springer-Verlag New York, Inc., Secaucus, NJ, USA 18, 19
- Mendonça PRS, Wong KYK, Cipolla R (2001) Epipolar geometry from profiles under circular motion. IEEE Trans Pattern Anal Mach Intell 23(6):604–616, DOI <http://dx.doi.org/10.1109/34.927461> 4
- Mikolajczyk K, Schmid C (2004) Scale and affine invariant interest point detectors. IJCV 60(1):63–86 2
- Mikolajczyk K, Schmid C (2005) A performance evaluation of local descriptors. IEEE Trans Pattern Anal Mach Intell 27(10):1615–1630 2
- Moravec HP (1977) Towards automatic visual obstacle avoidance. In: Proc. of the 5th International Joint Conference on Artificial Intelligence, p 584 2
- Moreels P, Perona P (2007) Evaluation of features detectors and descriptors based on 3d objects. Int J Comput Vision 73(3):263–284, DOI <http://dx.doi.org/10.1007/s11263-006-9967-1> 3
- Ohta Y, Kanade T (1985) Stereo by intra- and inter-scanline search using dynamic programming. IEEE Trans Pattern Analysis and Machine Intelligence 7(2):139–154 4
- Papadopoulos T (1996) Motion analysis of 3D rigid curves from monocular image sequences. Tech. Rep. RR-2779 (PhD Thesis), INRIA 4, 5, 18, 23, 24, 25
- Papadopoulos T, Faugeras OD (1996) Computing structure and motion of general 3D curves from monocular sequences of perspective images. In: Proceedings of the 4th European Conference on Computer Vision, Springer-Verlag, London, UK, pp 696–708 5, 18, 23, 24, 25
- Pollefeys M, Van Gool L, Vergauwen M, Verbiest F, Cornelis K, Tops J, Koch R (2004) Visual modeling with a hand-held camera. International Journal of Computer Vision 59(3):207–232, DOI <http://dx.doi.org/10.1023/B:VISI.0000025798.50602.3a> 3
- Ponce J, Genc Y (1998) Epipolar geometry and linear subspace methods: a new approach to weak calibration. International Journal of Computer Vision 28(3):223–243 20
- Porrill J, Pollard S (1991) Curve matching and stereo calibration. Image and Vision Computing 9(1):45–50, DOI [http://dx.doi.org/10.1016/0262-8856\(91\)90048-T](http://dx.doi.org/10.1016/0262-8856(91)90048-T) 4
- Pötsch K, Pinz A (2011) 3D geometric shape modeling by ‘3D contour cloud reconstruction from stereo videos. In: 16th Computer Vision Winter Workshop, Citeseer, p 99 3, 4

- Rao D, Chung SJ, Hutchinson S (2012) CurveSLAM: An approach for vision-based navigation without point features. In: IEEE/RSJ Intelligent Robots and Systems (IROS), pp 4198–4204, DOI 10.1109/IROS.2012.6385764 4
- Restrepo MI, Ulusoy AO, Mundy JL (2014) Evaluation of feature-based 3-D registration of probabilistic volumetric scenes. *ISPRS Journal of Photogrammetry and Remote Sensing* 98:1–18 3
- Reyes L, Bayro Corrochano E (2005) The projective reconstruction of points, lines, quadrics, plane conics and degenerate quadrics using uncalibrated cameras. *Image and Vision Computing* 23(8):693–706 4
- Robert L, Faugeras OD (1991) Curve-based stereo: figural continuity and curvature. In: *Proceedings of Computer Vision and Pattern Recognition*, pp 57–62 4, 13, 17
- Schmid C, Zisserman A (2000) The geometry and matching of lines and curves over multiple views. *International Journal of Computer Vision* 40(3):199–233, DOI <http://dx.doi.org/10.1023/A:1008135310502> 4
- Schneevoigt T, Schroers C, Weickert J (2014) A dense pipeline for 3d reconstruction from image sequences. In: *Pattern Recognition*, Springer, pp 629–640 20
- Seitz S, Curless B, Diebel J, Scharstein D, Szeliski R (2006) A comparison and evaluation of multi-view stereo reconstruction algorithms. In: *Proceedings of the IEEE Computer Society Conference on Computer Vision and Pattern Recognition*, IEEE Computer Society, pp 519–528 3
- Shashua A (1994) Trilinearity in visual recognition by alignment. In: *Proceedings of the third European conference on Computer vision*, Springer-Verlag, Secaucus, NJ, USA, pp 479–484 4
- Sherman D, Peleg S (1990) Stereo by incremental matching of contours. *IEEE Trans on Pattern Analysis and Machine Intelligence* 12(11):1102–1106, DOI <http://dx.doi.org/10.1109/34.61711> 4
- Shinozuka Y, Saito H (2014) Sharing 3D object with multiple clients via networks using vision-based 3D object tracking. In: *Proceedings of the 2014 Virtual Reality International Conference*, ACM, New York, NY, USA, VRIC '14, pp 34:1–34:4, DOI 10.1145/2617841.2620723, URL <http://doi.acm.org/10.1145/2617841.2620723> 3
- Simoes F, Almeida M, Pinheiro M, dos Anjos R (2012) Challenges in 3D reconstruction from images for difficult large-scale objects. *2014 XVI Symposium on Virtual and Augmented Reality* 0:74–83, DOI <http://doi.ieeecomputersociety.org/10.1109/SVR.2012.5> 3
- Sinha SN, Pollefeys M, McMillan L (2004) Camera network calibration from dynamic silhouettes. In: *Proceedings of the IEEE Computer Society Conference on Computer Vision and Pattern Recognition*, IEEE Computer Society, pp 195–202 4
- Spetsakis M, Aloimonos JY (1991) A multi-frame approach to visual motion perception. *Int J Comput Vision* 6(3):245–255, DOI <http://dx.doi.org/10.1007/BF00115698> 4
- Stewénius H, Engels C, Nistér D (2007) An efficient minimal solution for infinitesimal camera motion. In: *Computer Vision and Pattern Recognition, 2007. CVPR'07. IEEE Conference on*, IEEE, pp 1–8 20
- Tamrakar A (2008) Image contour extraction using geometric consistency. Ph.D. dissertation, Division Of Engineering, Brown University, Providence, RI, 02912 27
- Tamrakar A, Kimia BB (2007) No grouping left behind: From edges to curve fragments. In: *(ICCV2007 2007)* 27
- Teney D, Piater J (2012) Sampling-based multiview reconstruction without correspondences for 3D edges. In: *Proceedings, IEEE, Washington, DC, USA, 3DIMPVT '12*, pp 160–167, DOI 10.1109/3DIMPVT.2012.28, URL <http://dx.doi.org/10.1109/3DIMPVT.2012.28> 3
- Tian TY, Tomasi C, Heeger DJ (1996) Comparison of approaches to egomotion computation. In: *Computer Vision and Pattern Recognition, 1996. Proceedings CVPR'96, 1996 IEEE Computer Society Conference on*, IEEE, pp 315–320 19
- Triggs B (1999) Differential Matching Constraints. In: *Proceedings of the IEEE International Conference on Computer Vision*, IEEE Computer Society Press, Kerkyra, Greece 18
- Usumezbas A, Fabbri R, Kimia BB (2016) From multiview image curves to 3d drawings. In: *Proceedings of the IEEE Conference on Computer Vision and Pattern Recognition*, IEEE Computer Society Press, Las Vegas, Nevada, USA, submitted 5, 29
- Valgaerts L, Bruhn A, Mainberger M, Weickert J (2012) Dense versus sparse approaches for estimating the fundamental matrix. *International Journal of Computer Vision* 96(2):212–234, DOI 10.1007/s11263-011-0466-7, URL <http://dx.doi.org/10.1007/s11263-011-0466-7> 20
- Vieville T, Faugeras O (1996) The First Order Expansion of Motion Equations in the Uncalibrated Case. *Computer Vision and Image Understanding* 64(1):128–146 18
- Viéville T, Faugeras OD (1995) Motion analysis with a camera with unknown, and possibly varying intrinsic parameters. In: *Computer Vision, 1995. Proceedings., Fifth International Conference on*, IEEE, pp 750–756 19
- Wang R, Choi J, Medioni G (2014) 3D modeling from wide baseline range scans using contour coherence. In: *Computer Vision and Pattern Recognition (CVPR), 2014 IEEE Conference on*, IEEE, pp 4018–4025 4
- Waxman AM, Ullman S (1985) Surface structure and three-dimensional motion from image flow kinematics. *International Journal of Robotics Research* 4(3):72–94 18, 19

- Wong KY, Cipolla R (2004) Reconstruction of sculpture from its profiles with unknown camera positions. *IEEE Transactions on Image Processing* 13(3):381–94
- Wong KYK, Mendonça PRS, Cipolla R (2001) Head model acquisition from silhouettes. In: Arcelli C, Cordella L, di Baja GS (eds) *IWVF*, Springer, Capri, Italy, pp 787–796
- Yi Ma SS, Jana Koseck (1998) Motion recovery from image sequences: Discrete viewpoint vs. differential viewpoint. In: *Proceedings of European Conference on Computer Vision*, Springer, Lecture Notes in Computer Science, vol 1407, p 337–20
- Zhang L (2013) Line primitives and their applications in geometric computer vision. PhD thesis, Department of Computer Science, Univ. 3
- Zhuang X, Haralick RM (1984) Rigid body motion and the optic flow image. In: *Proceedings of the First Conference on Artificial Intelligence Applications*, IEEE Computer Society, pp 366–375
- Zucker S (2014) Stereo, shading, and surfaces: Curvature constraints couple neural computations. *Proceedings of the IEEE* 102(5):812–829